NASA TECHNICAL NOTE

NASA TN D-8264

A HIGH SUBSONIC SPEED WIND-TUNNEL INVESTIGATION OF WINGLETS ON A REPRESENTATIVE SECOND-GENERATION JET TRANSPORT WING

*Stuart G. Flechner, Peter F. Jacobs,
and Richard T. Whitcomb*

*Langley Research Center
Hampton, Va. 23665*

1. Report No. NASA TN D-8264	2. Government Accession No.	3. Recipient's Catalog No.
4. Title and Subtitle A HIGH SUBSONIC SPEED WIND-TUNNEL INVESTIGATION OF WINGLETS ON A REPRESENTATIVE SECOND-GENERATION JET TRANSPORT WING		5. Report Date July 1976
		6. Performing Organization Code
7. Author(s) Stuart G. Flechner, Peter F. Jacobs, and Richard T. Whitcomb		8. Performing Organization Report No. L-10387
		10. Work Unit No. 505-11-11-04
9. Performing Organization Name and Address NASA Langley Research Center Hampton, Va. 23665		11. Contract or Grant No.
		13. Type of Report and Period Covered Technical Note
12. Sponsoring Agency Name and Address National Aeronautics and Space Administration Washington, D.C. 20546		14. Sponsoring Agency Code

15. Supplementary Notes

16. Abstract

This paper discusses the effects of winglets (described in NASA TN D-8260) on the aerodynamic forces and moments, loads, and crossflow velocities behind the wing tip. The results of the investigation indicate that winglets significantly reduce the drag coefficient at lifting conditions. The experiments were conducted in the Langley 8-foot transonic pressure tunnel at Mach numbers from 0.70 to 0.83 and over a lift coefficient range up to 0.65. A semispan model was used.

17. Key Words (Suggested by Author(s)) Winglets Induced drag Drag due to lift	18. Distribution Statement Unclassified — Unlimited Subject Category 02

19. Security Classif. (of this report) Unclassified	20. Security Classif. (of this page) Unclassified	21. No. of Pages 66	22. Price* $4.25

A HIGH SUBSONIC SPEED WIND-TUNNEL INVESTIGATION
OF WINGLETS ON A REPRESENTATIVE
SECOND-GENERATION JET
TRANSPORT WING

Stuart G. Flechner, Peter F. Jacobs,
and Richard T. Whitcomb
Langley Research Center

SUMMARY

This paper presents the effects of winglets (described in NASA TN D-8260) on the aerodynamic forces and moments, loads, and crossflow velocities behind the wing tip of a representative second-generation jet transport wing. The investigation was conducted in the Langley 8-foot transonic pressure tunnel using a semispan model. The test was carried out at Mach numbers of 0.70, 0.80, and 0.83 over a lift coefficient range up to 0.65, and at a constant Reynolds number of 13.1×10^6 per meter (4.0×10^6 per foot).

The results of the investigation indicate that winglets significantly reduce the induced drag coefficient with a resulting 0.0015 reduction in overall drag coefficient at the design condition at a Mach number of 0.80 and a lift coefficient of 0.53. The winglets cause small increases in the lift coefficients and produce small negative increments in the pitching-moment coefficients at near-design conditions. The bending-moment coefficients at the wing-fuselage juncture are increased slightly because of (1) the increased lift loads on the wing at the tip and (2) the substantial side loads on the upper winglet. The winglets substantially reduce the magnitudes of the crossflows behind the wing tip. When compared with wing-tip extensions on the basis of equal effects on wing bending-moment coefficients, winglets produce substantially greater reductions in the drag coefficients at near-design conditions.

INTRODUCTION

Winglets, described in reference 1, are intended to provide reductions in drag coefficient for near-cruise conditions substantially greater than those obtained with simple wing-tip extensions which impose the same bending-moment increments on the wing structure. The National Aeronautics and Space Administration has been conducting extensive experimental investigations of the effects of winglets for jet transport wings at high subsonic Mach numbers, and this report is the first to document these studies.

The investigation reported here was conducted to determine the effects of winglets on the aerodynamic forces and moments, loads, and crossflow velocities behind the wing tip for a representative second-generation transport wing. In an effort to obtain the highest winglet Reynolds number, a semispan model was used. The investigation was conducted in the Langley 8-foot transonic pressure tunnel. The tests were carried out at Mach numbers of 0.70, 0.80, and 0.83 for lift coefficients up to 0.65. A constant Reynolds number of 13.1×10^6 per meter $(4.0 \times 10^6$ per foot) was maintained.

The effects of winglets on the longitudinal and directional aerodynamic characteristics of a representative second-generation jet transport are presented in reference 2. That study used a full-span model without tails.

SYMBOLS

The longitudinal aerodynamic characteristics presented in this report are referred to the stability-axis system. Force and moment data have been reduced to coefficient form based on the exposed area of the basic wing. All dimensional values are given in both International System of Units (SI) and U.S. Customary Units. (See ref. 3.) All measurements and calculations were made in U.S. Customary Units.

Coefficients and symbols used herein are defined as follows:

A aspect ratio of basic wing, based on original wing outer panel extended to plane of symmetry, $(\text{Span})^2/\text{Area}$, 7.13

$b/2$ exposed semispan of wing with basic tip, 136.53 cm (53.75 in.)

$C_{B,w}$ bending-moment coefficient of wing at wing-fuselage juncture,

$$\frac{\text{Bending moment}}{q_\infty S \frac{b}{2}}$$

$C_{B,y'}$ bending-moment coefficient for spanwise station y',

$$C_{B,y'} = \frac{1}{S\frac{b}{2}} \int_{y'}^{b/2} c_n c(y - y') \, dy$$

$\Delta C_{B,y'}$ incremental change in bending-moment coefficient at y',

$$\left(C_{B,y'}\right)_{\text{winglets on or tip extension on}} - \left(C_{B,y'}\right)_{\text{basic tip}}$$

2

C_D drag coefficient, $\dfrac{\text{Drag}}{q_\infty S}$

$C_{D,i}$ induced drag coefficient

ΔC_D incremental drag coefficient, $\left(C_D\right)_{\text{winglets on}} - \left(C_D\right)_{\text{basic tip}}$

C_L lift coefficient, $\dfrac{\text{Lift}}{q_\infty S}$

C_m pitching-moment coefficient about moment reference center,

$$\dfrac{\text{Pitching moment}}{q_\infty S \bar{c}}$$

$C_{N,\text{upper winglet}}$ force coefficient, normal to upper winglet, obtained by integrating upper winglet spanwise load distribution

C_p pressure coefficient, $\dfrac{p_l - p_\infty}{q_\infty}$

$C_{p,\text{sonic}}$ pressure coefficient corresponding to local speed of sound

c local chord, cm   (in.)

$\bar{c}$ mean geometric chord of exposed basic wing, 44.30 cm (17.44 in.)

c_{av} average chord of exposed basic wing, $\dfrac{S}{b/2}$, 42.08 cm (16.57 in.)

c_n section normal-force coefficient obtained from integrated pressure measurements

c_y section side-force coefficient obtained from c_n

h vertical height above wing tip (see fig. 2(b)), cm   (in.)

M_∞ free-stream Mach number

p_l local static pressure, N/m^2 (lb/ft^2)

p_∞ free-stream static pressure, N/m^2 (lb/ft^2)

q_∞ free-stream dynamic pressure, N/m^2 (lb/ft^2)

S   area of exposed basic wing, $0.5745 \ m^2$ $(6.1837 \ ft^2)$

x   chordwise distance aft of leading edge, cm (in.)

y   spanwise distance from wing-fuselage juncture, positive outboard, cm (in.)

y'   spanwise station at which bending-moment coefficient is determined, cm (in.)

α angle of attack, deg

Abbreviations:

L.S.   lower surface

U.S.   upper surface

EXPERIMENTAL APPARATUS AND PROCEDURES

Test Facility

This investigation was conducted in the Langley 8-foot transonic pressure tunnel, a continuous, single-return tunnel with a slotted, rectangular test section. The longitudinal slots in the floor and ceiling of the test section reduce tunnel wall interference and allow relatively large models to be tested through the subsonic speed range. Controls are available to permit independent variation of Mach number, stagnation pressure, temperature, and dewpoint. A more detailed description of the tunnel is found in reference 4.

Model Description

In an effort to obtain the highest winglet Reynolds number and a sufficient winglet size in which to install surface-pressure measurement tubes, a semispan model was used. Photographs of the model in the wind tunnel are shown in figure 1. Drawings of the model are shown in figure 2. The model fuselage and wing approximate those of a representative second-generation jet transport. No tail surfaces were simulated.

Fuselage.- The fuselage has an elliptical nose, a cylindrical midsection, and a boat-tail afterbody. The midsection covered the balance and had a slot through which the wing protruded. The fuselage was not attached to the balance but did rotate with the wing through the angle-of-attack range.

4

Wing.- The basic wing used in this investigation has advanced peaky airfoil sections (fig. 2(c)) and approximately an elliptical span load distribution at the design condition of $M_\infty = 0.80$ and $C_L = 0.53$. This wing has 6° dihedral, a root chord incidence of 5.9°, and a twist that varies from 3.6° (washout) at the trailing-edge break station to 9.4° (washout) at the tip. The outboard region has a quarter-chord sweep of 35° and a constant 10 percent thickness ratio. The trapezoidal planform, excluding the inboard trailing-edge extension region but including the wing portion within the fuselage, has an aspect ratio of 7.13 and a taper ratio of 0.228. For data analysis purposes (reference area S, semispan b/2, mean geometric chord $\bar{c}$, average chord c_{av}), only the exposed region of the basic wing, including the inboard trailing-edge extension region, was considered. A small portion, 0.025b/2 of the tip of the basic wing, was removed before adding the winglets to reduce the increased bending moments in the wing associated with adding the winglets. (See fig. 2.) The amount removed approximates the portion of the wing outboard of the main wing structural box for the jet transport configuration simulated for this investigation.

Winglets.- A detailed drawing of the winglets is given in figure 2(b). The winglets employed modified 11-percent-thick supercritical airfoil sections (fig. 2(c)) and a total area of 2.5 percent of the basic wing exposed area. The ratios of winglet average chord to wing average chord are 0.16 and 0.12 for the upper and lower winglets, respectively.

The upper winglet has a span approximately equal to the wing-tip chord, a root chord equal to 60 percent of the wing-tip chord, a taper ratio of 0.39, and a leading-edge sweep of 38°. This upper winglet is canted outward 18° from the vertical (72° dihedral) and toed out 2° (leading edge outboard) relative to the fuselage center line and is untwisted; as a result, the geometric incidence is constant and negative. The airfoil "upper surface" is the inboard surface. The lower winglet, whose span must be shorter to allow for ground clearance, has a root chord equal to 40 percent of the wing-tip chord, a taper ratio of 0.60, and a leading-edge sweep of 52° (fig. 2(b)). This lower winglet is canted outward 36° from the vertical (54° anhedral) and toed in 6.5° at the root, relative to the fuselage center line, with 1.5° washout at the tip. The upper surface of this winglet is the outboard surface. The planform and the magnitudes of the toe-in, twist, and cant for this lower winglet have not been optimized.

To make the transition smoothly from the wing to the winglets, fillets were added to the inside corners at those junctures, and the outside corners were rounded.

Vortex generator.- To alleviate a local separation problem between the wing upper surface and the upper winglet, a small, cambered vortex generator was added to the wing upper surface. (See fig. 2(a).) The vortex generator is 1.19 cm (0.47 in.) at the base, 0.25 cm (0.10 in.) at the tip, and 0.81 cm (0.32 in.) in height. The leading edge was swept back 49.1°. The vortex generator was located 1.65 cm (0.65 in.) inboard of the wing-

winglet juncture with the trailing edge 2.79 cm (1.10 in.) ahead of the wing trailing edge and was approximately parallel with the airstream.

Boundary-Layer Transition Strips

Boundary-layer transition strips were placed on the upper and lower surfaces of the wing and winglets. These strips were comprised of a 0.16-cm (0.06-in.) wide band of carborundum grains set in a plastic adhesive. The carborundum grains were sized by following the procedure of reference 5. The transition pattern for the wing is shown in figure 3.

On the lower surface (outboard) of the upper winglet, No. 120 grains were applied at the 40-percent chord line. No. 150 grains were applied on the upper surface (inboard) from a point 2.54 cm (1.0 in.) from the leading edge at the root to a point 0.89 cm (0.35 in.) from the leading edge at the mid-semispan station. No. 180 grains were applied from that point to a point 0.25 cm (0.10 in.) from the leading edge at the tip of the winglet. On the lower winglet, No. 240 grains were applied at 5 percent of the stream-wise chord of the upper surface (outboard), and No. 220 grains were applied at the 40-percent chord line for the lower surface (inboard).

The transition strips on the lower surface of the winglets were located rearward in an attempt to simulate full-scale Reynolds number boundary-layer conditions (ref. 6). The strips on the upper surface of the winglets were located forward to insure transition ahead of the shock for the various test conditions.

Test Conditions

Measurements were taken at Mach numbers of 0.70, 0.80, and 0.83 with the angle of attack of the model ranging from approximately -3° to 7°. Stagnation temperature was maintained at 322 K (120° F) throughout the entire test, and the air dried until the dewpoint was sufficiently low to prevent condensation effects. A constant Reynolds number of 13.1×10^6 per meter (4.0×10^6 per foot) was maintained for this investigation. The free-stream dynamic pressures q_∞ for the three test Mach numbers were 28.6, 31.6, and 32.4 kN/m^2 (597, 660, and 677 lb/ft^2), respectively.

Measurements

Force and moment data were obtained by using a five-component electrical strain-gage balance. Side-force measurements were not taken. The angle of attack was measured within the fuselage.

Chordwise static-pressure distributions were measured at the 0.261, 0.907, and 0.963 semispan stations on the basic wing. In addition, they were measured at three stations on the upper winglet for the wing plus winglets configuration. These stations

6

were at 0.22, 0.50, and 0.78 of the upper winglet span. The stations are located at the 0.991, 1.003, and 1.015 wing semispan stations. (Note that semispan stations are defined as a fraction of the distance from the wing-fuselage juncture to the tip of the basic wing. Because the upper winglet extends beyond this distance, semispan stations can be greater than 1.0.)

A special sting-mounted yaw head rake was used to survey the flow field behind the wing-tip configurations (fig. 4). Details of the yaw head rake are given in reference 7. The rake was located approximately two wing-tip chords behind the wing trailing edge with the center slightly above and inboard of the wing tip. Data were taken with the rake located in the vertical, horizontal, and ±45° positions for both wing-tip configurations.

Corrections

The angle of attack of the model was corrected for flow angularity in the wind tunnel. The slotted wind-tunnel test section reduces wall effects on lift; therefore, no correction was made to the data for this effect. The wing semispan and the model frontal area were sufficiently small so that corrections to Mach number for wind-tunnel blockage effects were unnecessary. The tip of the wing was approximately 50.8 cm (20 in.) from the tunnel sidewall. This distance corresponds to about three spans of the upper winglet. Thus, the influence of the wall on the winglet loads should be small.

The yaw head rake was placed at an angle of attack of 1.8° during the investigation. This position properly located the rake in the area of interest behind the model. Corrections to the yaw head rake calibration were made to account for this initial angle.

Validity of Data

To insure the validity of the balance data presented, particularly the drag increments caused by the winglets, two tests were made for each tip configuration discussed in this paper. At the design condition, $M_\infty = 0.80$ and $C_L = 0.53$, the difference between the drag coefficients for the two tests of a given configuration was about 0.0002. The lift coefficient differed by less than 0.2 percent for the two tests of a given configuration at the design condition. These increments provide an indication of the repeatability of the data. The data for the two configurations shown in figures 5, 6, and 7 are averages of the results for the two tests for each configuration.

PRESENTATION OF RESULTS

The figures presented in the following list contain the results of this investigation. All of the results presented in the report are not discussed in "Results and Discussion." Those not discussed are included for reference purposes.

RESULTS AND DISCUSSION

Force and Moment Characteristics

Drag.- The configuration used in this investigation results in unrepresentative absolute axial-force values since there is substantial drag associated with the gap between the wing and fuselage. The gap effects can reasonably be considered systematic and will thus affect all configurations equally at the same test conditions. Both lift and drag values are influenced by the gap effects on axial force. For this limited angle-of-attack range, however, the lift component of axial-force error is a negligible percentage of the total lift, but the drag component of axial-force error is a considerable percentage of the total drag. Therefore, absolute values of lift are presented while the drag results are given as a plot of incremental drag coefficient due to adding the winglets to the basic wing configuration plotted against lift coefficient. (See fig. 5.)

As expected, the added skin friction and form drag of the winglets predominate at low lift coefficients. At a near-design lift coefficient of 0.53, the winglets have reduced the induced drag so that there are incremental drag-coefficient reductions of 0.0012, 0.0015, and 0.0020 for Mach numbers of 0.70, 0.80, and 0.83, respectively. As the lift coefficient of the wing is increased further, the favorable effects of the winglets increase. The selected design lift coefficient of 0.53 is based on the exposed wing area and corre-

sponds to an overall trimmed airplane lift coefficient of about 0.48. It should also be noted that with winglets installed, the optimum cruise lift coefficient for an airplane would increase by about 6 or 7 percent as a result of the rotation of the drag coefficient plotted against the lift-coefficient polar associated with the addition of the winglets. Thus, this selected design lift coefficient corresponds to an unmodified airplane lift coefficient of 0.45 which is near the cruise lift coefficients for present jet transports.

At full-scale Reynolds numbers, the skin-friction drag of the winglets would be significantly less than at the Reynolds numbers of this investigation; for such conditions the favorable increments caused by these surfaces would be greater than those measured. It has been estimated that the increment is about 0.0002.

The reductions of induced drag caused by the addition of winglets are greater than the reductions in the increment of measured total drag (fig. 5) because of the increase in skin friction and form drags associated with adding winglets. It has been estimated that for the design condition of $M_\infty = 0.80$ and $C_L = 0.53$, these effects add a C_D increment of about 0.0003. Thus, for this condition the reduction in induced drag coefficient must be about 0.0018. A comparison of this increment with the estimated induced drag coefficient for the wing $\left(C_{D,i} = \dfrac{C_L{}^2}{0.95\pi A} \right)$ suggests that the winglets reduce the induced drag for this condition by about 13 percent. When the theoretical effect of the cant or dihedral of the winglets is included, this increment is approximately the same as the calculated effects of references 8 and 9 for vertical surfaces with the same ratio of total height to wing semispan as that for the present configuration.

The reductions in drag coefficient achieved during this investigation are substantially less than those obtained for the configuration of reference 1 for comparable lift coefficients. The differences can be attributed primarily to the smaller relative winglet height for the present investigation. The differences also result from the removal of part of the basic wing span before the winglets were added during the present investigation.

Lift and pitching moment.- Figure 6 shows that the winglets produce small increases in the model lift coefficients.

Figure 7 shows that at the cruise lift coefficient of 0.53, the pitching-moment coefficient is 0.008 more negative with the winglets on. This change corresponds approximately to a shift in center of pressure equal to 1.5 percent of the mean geometric chord. Calculations indicate that the change should increase the trim drag coefficient less than 0.0001. There was a small positive change in the zero-lift pitching-moment coefficient $\left(C_{m,o} \right)$ caused by the addition of the winglets since the winglets reduce the lift at the wing tip for low lift coefficients. The addition of the winglets had an insignificant effect on the "pitch-up" characteristics of the wing.

Wing bending moments.- As shown in figure 7, the winglets increase the wing bending-moment coefficient at the wing-fuselage juncture by no more than 2 percent for lift coefficients up to 0.6. At the design condition of $M_\infty = 0.80$ and $C_L = 0.53$, this bending-moment coefficient is increased by only 1.4 percent. For the configuration of reference 1, this bending-moment coefficient was increased by about 3.5 percent. The difference exists primarily because, for this investigation, part of the wing tip was removed before the winglets were added.

Loads

Wing and winglet pressure coefficients.- The pressure data measured on the model are presented in figure 8. The first three upper surface orifices of the upper winglet pressure row at $\frac{y}{b/2} = 0.991$ (near winglet root) were damaged during the investigation and were not used. To provide a reasonable pressure distribution for integration purposes, the pressure coefficient at $\frac{x}{c} = 0.02$ for $\frac{y}{b/2} = 1.003$ was used for the three missing coefficients and is presented as a dashed line. The distributions of pressure are typical of those for supercritical airfoils.

The inboard wing station $\left(\text{fig. 8, } \frac{y}{2/b} = 0.261\right)$ shows essentially no effect resulting from the addition of the winglets. At the wing station of $\frac{y}{b/2} = 0.907$, the pressure coefficients over the rear portion of the upper surface of the wing are slightly more negative under the influence of the upper winglet. The outboard wing station $\left(\frac{y}{b/2} = 0.963\right)$ shows a much larger negative increment in the aft pressure coefficients, a result of the presence of the upper winglet. The influence of the lower, forward winglet can be seen in the increase in the pressure coefficient in the 20- to 50-percent chord region. The second pressure peak at 65-percent chord is approximately opposite the 35-percent chord peak measured on the winglet at station 0.991. $\left(\text{Note that the tick mark at } \frac{x}{c} = 0.52 \left(\frac{y}{b/2} = 0.963\right)\right.$ represents the projection of the upper winglet leading-edge intersection with the wing tip.$\Big)$

Spanwise loadings.- Figure 9 shows the load distributions across the wing span. The section normal-force coefficient, weighted by c/c_{av}, is presented against exposed wing semispan location where 0 is the wing-fuselage juncture and 1.0 is the end of the wing with the basic tip. The curve shown in the figures represents an elliptical load distribution which is forced to go through the measured data point for the basic wing-tip configuration at semispan station 0.261 and through a zero load point at the tip. The figure also shows the section side-force coefficient of the upper winglet, also weighted, presented

against the vertical height along the winglet. The section normal-force coefficients for the lower winglet are unknown.

The data show that the basic wing-tip configuration has reasonably good load distributions, essentially elliptical at and near the design condition of $M_\infty = 0.80$ and $C_L = 0.53$. The addition of the winglets results in a significant increase in the section load at the outboard measurement station $\left(\dfrac{y}{b/2} = 0.963\right)$ but relatively little change in the loads at the $\dfrac{y}{b/2} = 0.907$ station. The measured increases in section loads on the outboard region of the wing are about one-half of those indicated as optimum in references 8 and 9. As noted in reference 1, such a variation from the theoretical optimum results in a significant reduction in the added bending moment imposed on the wing structure. For near-design conditions the loads on the upper winglet are about two-thirds of those indicated as optimum in references 8 and 9.

Ratios of the normal-force coefficients for the upper winglet to the total lift coefficients are presented in figure 10. At near-design lift coefficients the normal-force coefficients for this surface are somewhat greater than the lift coefficients.

Downstream Crossflows and Discussion of Phenomena

The crossflow velocity vectors measured behind the wing with the basic tip and the winglets added are presented in figure 11. The vectors for the configuration with the basic wing-tip configuration suggest a typical vortex circulation. The center of this circulation appears to be inboard from the tip and above the wing as indicated by the cross. Unpublished data taken in the vortex research facility at the Langley Research Center and photographs of smoke emitted from the tip of a transport aircraft in flight confirm that the wing-tip vortex core rises above the wing before finally moving down.

The addition of the winglets spreads the vorticity behind the tip to such an extent that a discrete vortex core is not apparent. The crossflow velocities in the region where the core had been located are as small as 25 percent of the former velocities. In particular, the winglets have drastically reduced the inflow above the wing. The upper winglet causes a small increase in the velocities, behind the tip of that surface.

Induced drag is, of course, directly related to the total energy of the crossflow circulation. Thus, the induced drag reduction caused by the addition of the winglets must result from a diminishing of this energy. (See ref. 10.) This energy reduction is associated primarily with the marked reduction of the measured high crossflow velocities near the vortex center for the configuration with the basic tip. Analyses indicate that the primary mechanism by which the reduction of the drag force on the model is accomplished is the forward inclination of the side-force vectors on the winglets resulting from the

local crossflows. The reduction is also conjectured to be caused by a small decrease in the downwash of the flow approaching the wing.

Comparisons With a Wing-Tip Extension

As indicated in the "Introduction," the primary objective of the research program on winglets is to achieve reductions in drag coefficient, at lifting conditions, substantially greater than those obtained with wing-tip extensions which impose the same bending-moment increments on the wing structures. In the present investigation no attempt was made to arrive experimentally at such a tip extension. However, calculations have been made to determine the approximate size and effect of such an extension at the design condition of $M_\infty = 0.80$ and $C_L = 0.53$. In these calculations, it has been assumed that the spanwise distribution of load on the wing with such an extension is the same as that without the extension, that is, essentially elliptical.

These calculations indicate that for the design condition, a tip extension of 1.5 percent of the reference semispan would produce approximately the same total bending-moment increments as those produced by the winglets. The bending-moment increments along the semispan caused by the addition of the winglets are compared with those for the 1.5-percent wing-tip extension in figure 12. After accounting for differences in skin friction and wing loading, this assumed tip extension would reduce the drag coefficient by about 0.0003 for the design condition compared with 0.0015 obtained with the winglets for the same condition. Hence, it is apparent that when compared on the basis of equal effects on wing bending-moment coefficients, winglets produce substantially greater reductions in the drag coefficients at near-design conditions than would a simple wing-tip extension.

It should be noted that the difference between the drag-coefficient reductions resulting from the addition of winglets and the reductions provided by a tip extension for equal total bending moments is markedly affected by the amount of span removed from the basic wing tip before adding the winglets. As indicated in the description of the model, 2.5 percent of the reference semispan was removed for the experiments described herein. Calculations similar to these just described indicate that if none of the wing tip had been removed before adding the winglets, the total bending moments would have been about the same as a 3.8-percent wing-tip extension. The drag coefficient reductions would have been about 0.0020 for the winglets and 0.0008 for the wing-tip extension. The ratio of these reductions is roughly the same as that determined experimentally for the configuration of reference 1.

Calculations indicate that the addition of a 1.5-percent semispan tip extension would increase the negative pitching-moment coefficient at the design condition by a greater increment than did the addition of the winglets (fig. 7).

CONCLUSIONS

The results of a high-speed wind-tunnel investigation of the effects of winglets on a representative second-generation jet transport wing indicate the following conclusions:

1. The winglets significantly reduce the induced drag coefficient with a resulting reduction in total drag coefficient of approximately 0.0015 at the design condition of a Mach number of 0.80 and a lift coefficient of 0.53.

2. The winglets produce small increases in the lift coefficients and small negative increments in the pitching-moment coefficients at the near-design conditions.

3. The winglets significantly increase the wing normal-force coefficient at the wing tip near the design lift coefficient. Also, the normal-force coefficients for the upper winglet are somewhat greater than the wing lift coefficients. These loads result in slight increases of the wing bending-moment coefficient at the wing-fuselage juncture: about 1.4 percent at the design condition.

4. The reductions in induced drag are associated with a spreading of the vortex crossflows behind the wing tip.

5. Theoretical calculations indicate that when compared on the basis of equal effects on wing bending-moment coefficients, winglets produce substantially greater reductions in the drag coefficients at near-design conditions than would a wing-tip extension.

Langley Research Center
National Aeronautics and Space Administration
Hampton, Va. 23665
June 1, 1976

REFERENCES

1. Whitcomb, Richard T.: A Design Approach and Selected Wind-Tunnel Results at High Subsonic Speeds for Wing-Tip Mounted Winglets. NASA TN D-8260, 1976.

2. Jacobs, Peter F.; and Flechner, Stuart G.: The Effect of Winglets on the Static Aerodynamic Stability Characteristics of a Representative Second-Generation Jet Transport Model. NASA TN D-8267, 1976.

3. Mechtly, E. A.: The International System of Units — Physical Constants and Conversion Factors (Second Revision). NASA SP-7012, 1973.

4. Schaefer, William T., Jr.: Characteristics of Major Active Wind Tunnels at the Langley Research Center. NASA TM X-1130, 1965.

5. Braslow, Albert L.; and Knox, Eugene C.: Simplified Method for Determination of Critical Height of Distributed Roughness Particles for Boundary-Layer Transition at Mach Numbers From 0 to 5. NACA TN 4363, 1958.

6. Blackwell, James A., Jr.: Preliminary Study of Effects of Reynolds Number and Boundary-Layer Transition Location on Shock-Induced Separation. NASA TN D-5003, 1969.

7. Patterson, James C., Jr.; and Flechner, Stuart G.: An Exploratory Wind-Tunnel Investigation of the Wake Effect of a Panel Tip-Mounted Fan-Jet Engine on the Lift-Induced Vortex. NASA TN D-5729, 1970.

8. Weber, J.: Theoretical Load Distribution on a Wing With Vertical Plates. R. & M. No. 2960, British A.R.C., 1956.

9. Lundry, J. L.: A Numerical Solution for the Minimum Induced Drag, and the Corresponding Loading, of Nonplanar Wings. NASA CR-1218, 1968.

10. Cone, Clarence D., Jr.: The Theory of Induced Lift and Minimum Induced Drag of Nonplanar Lifting Systems. NASA TR R-139, 1962.
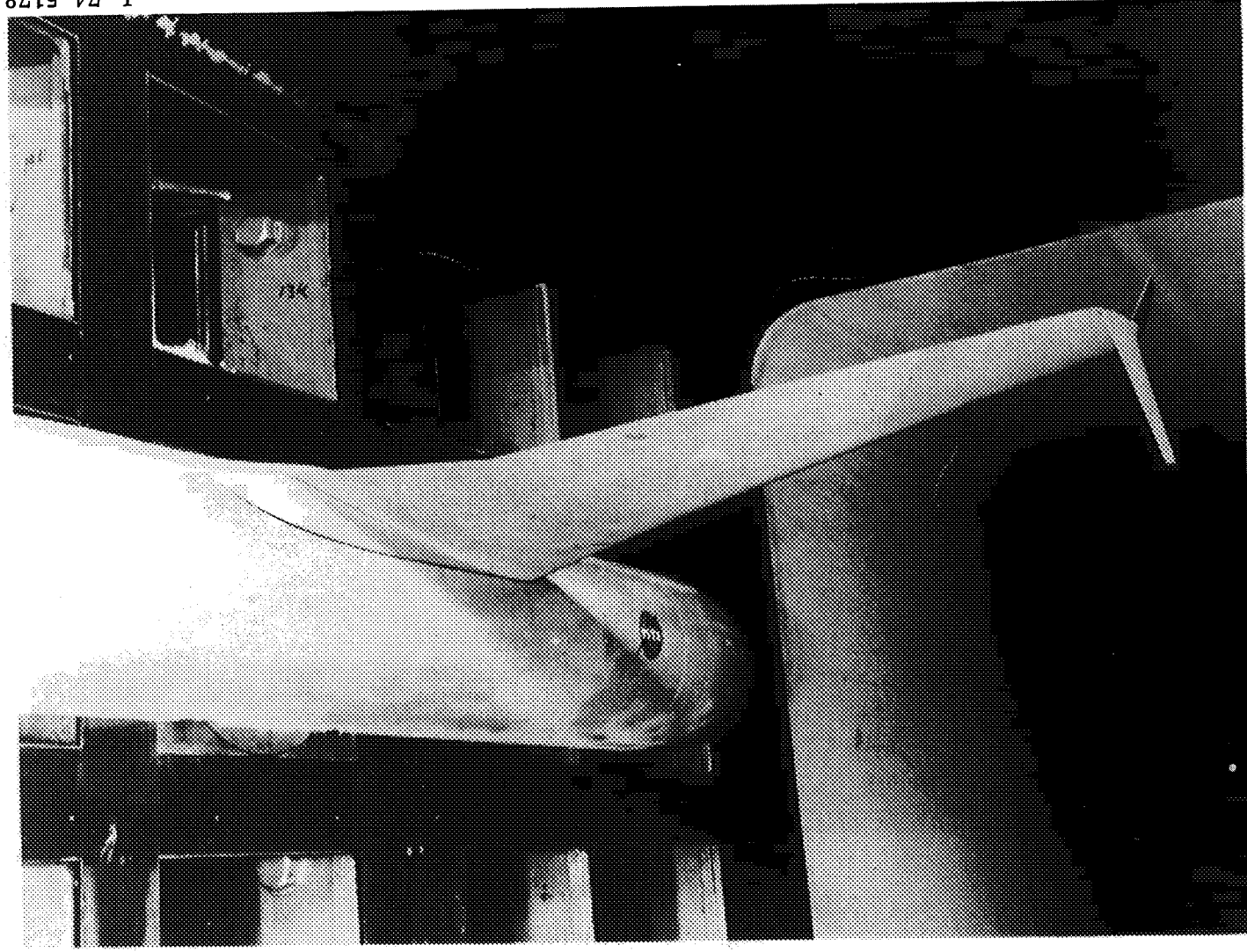
(a) Winglet semispan model.

Figure 1.- Model photographs.

L-74-5178
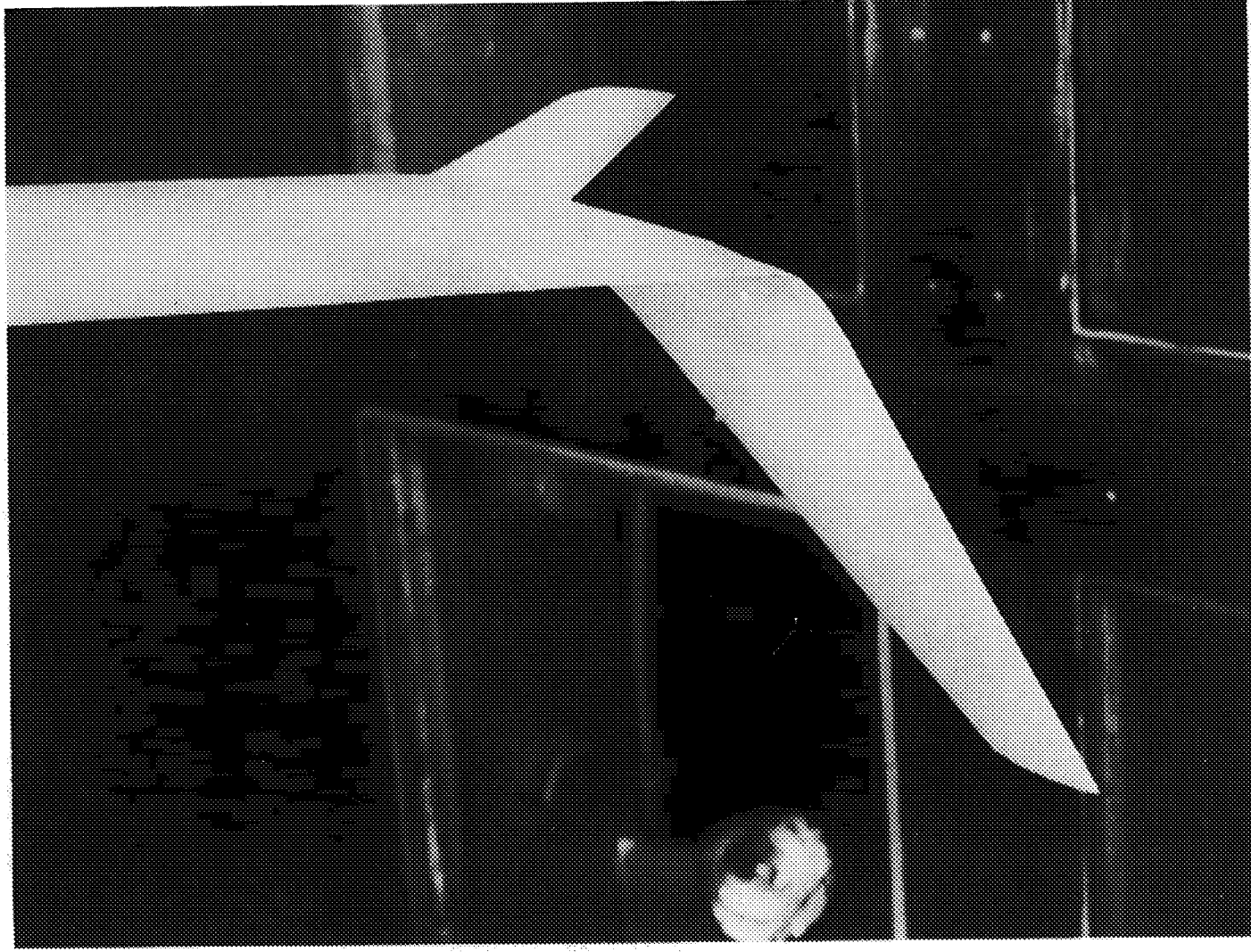
(b) Closeup of winglets.

Figure 1.- Concluded.

L-74-6196

99.09(39.01) ─── 71.32(28.08) ──

Spacer

75.44(29.70)

166.85(65.69)

Vortex generator

.81(.32)

1.27(.50)

2.79(1.10)

Wing upper surface

1.19(.47)

Trailing edge

View A─A

35°

c/4

136.53(53.75)

A A

Basic tip

3.43(1.35)

16.26(6.40)

320.04(126.00)

Moment reference center

Radius=19.68(7.75)
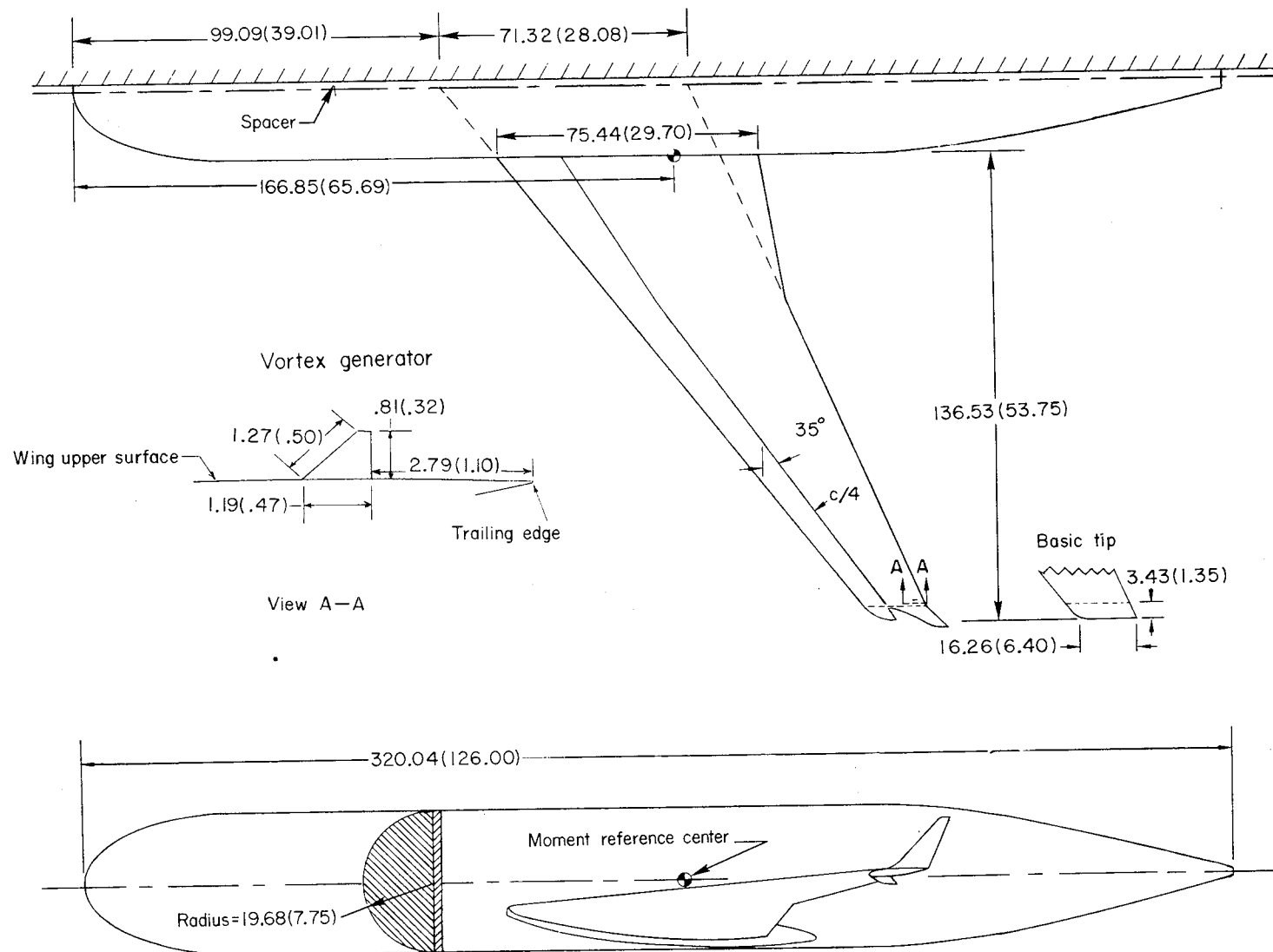
(a) General layout of model.

Figure 2.- Drawing of winglet model. All dimensions are in centimeters (inches).

18

Section A–A

3.8(1.5)

3.3(1.3)

38°

19.1(7.5)

9.7(3.8)

h=0

6.4(2.5)

52°

3.8(1.5)

A

h

18°

36°

6° dihedral

A
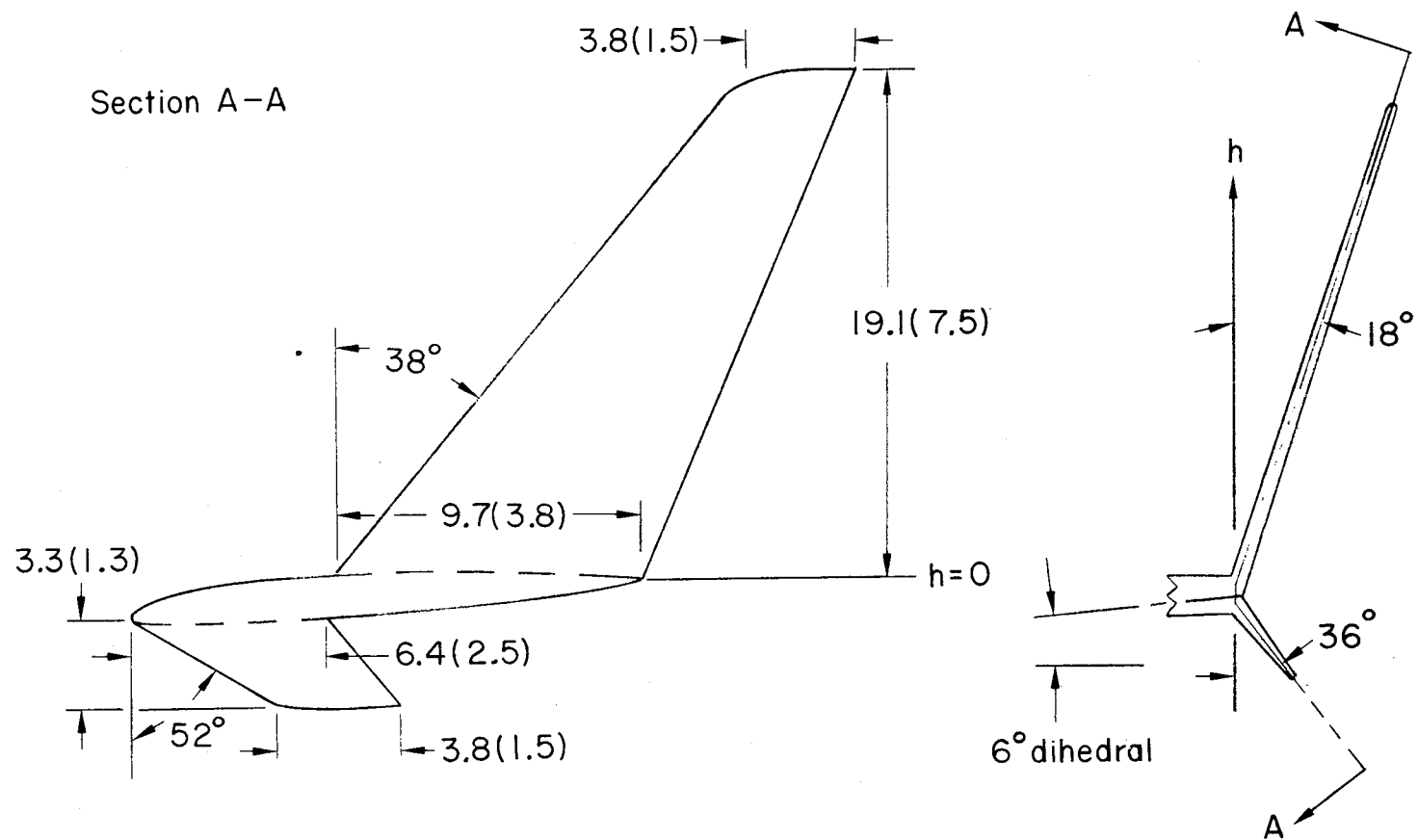
(b) Winglet details.

Figure 2.- Continued.

Upper winglet - midspan

Wing —— $\dfrac{y}{b/2} = 0.970$
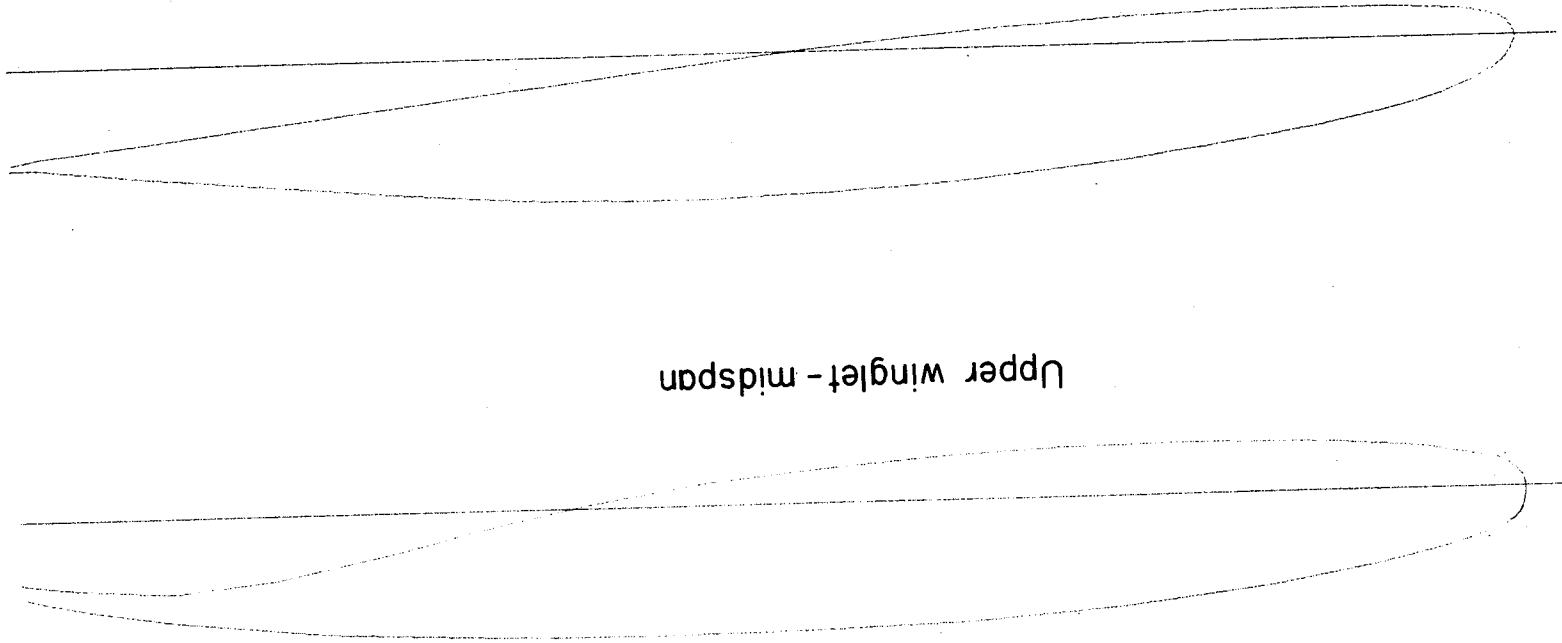
(c) Upper winglet and wing airfoil shapes in percent local chord.

Figure 2.- Concluded.

Wing-fuselage juncture

.15c

Grain size
No. 100

No.120

Grain size
No. 100

No.120

60.96 (24.0)

45.72
(18.0)

No. 120

No. 150

.06 c

Upper
surface

.15c

.10 c

Lower
surface

8.25
(3.25)
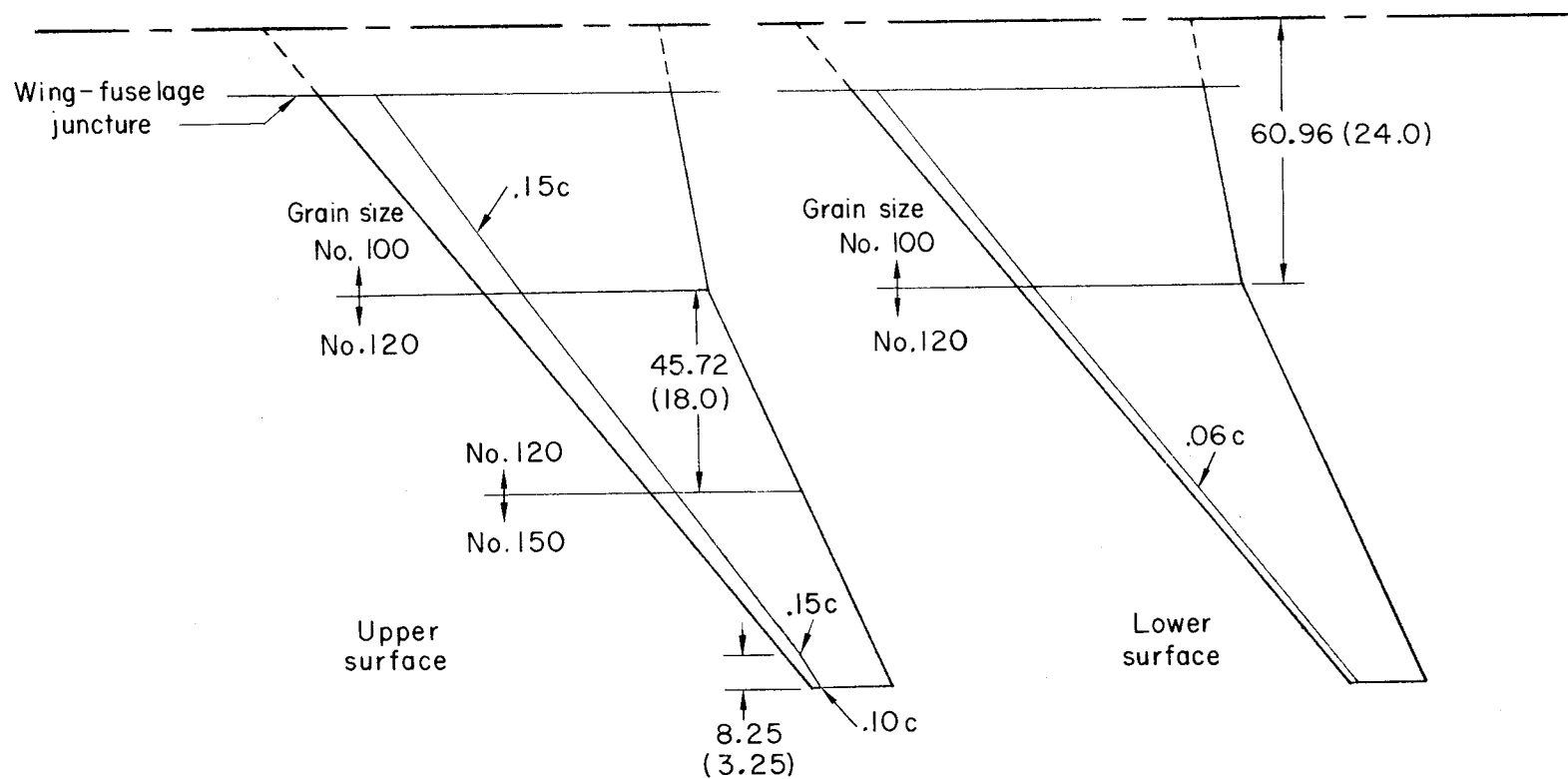
Figure 3.- Details of wing boundary-layer transition-strip patterns.
All dimensions are in centimeters (inches).
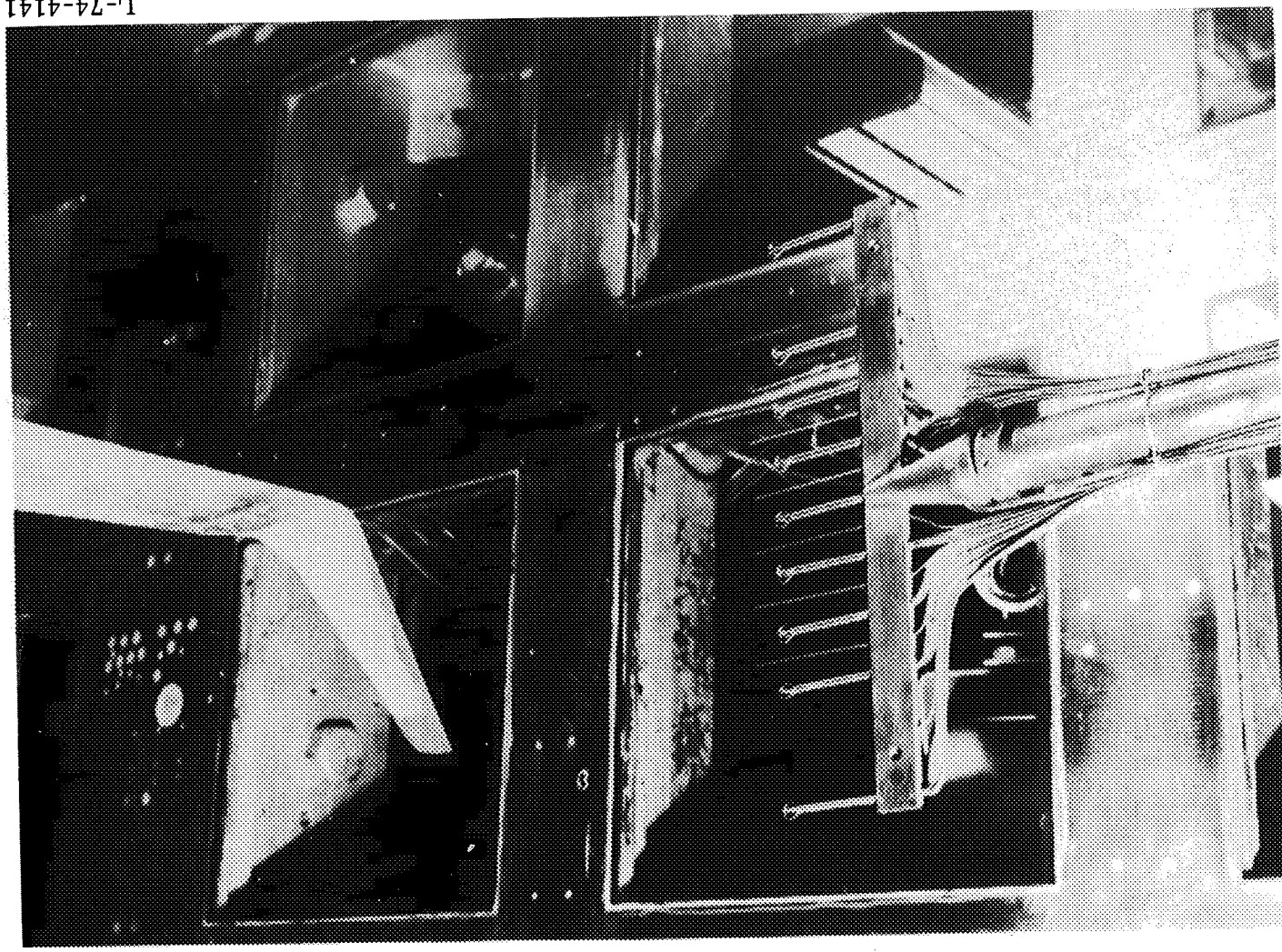
Figure 4.- Photograph of yaw head rake behind model.

L-74-4141
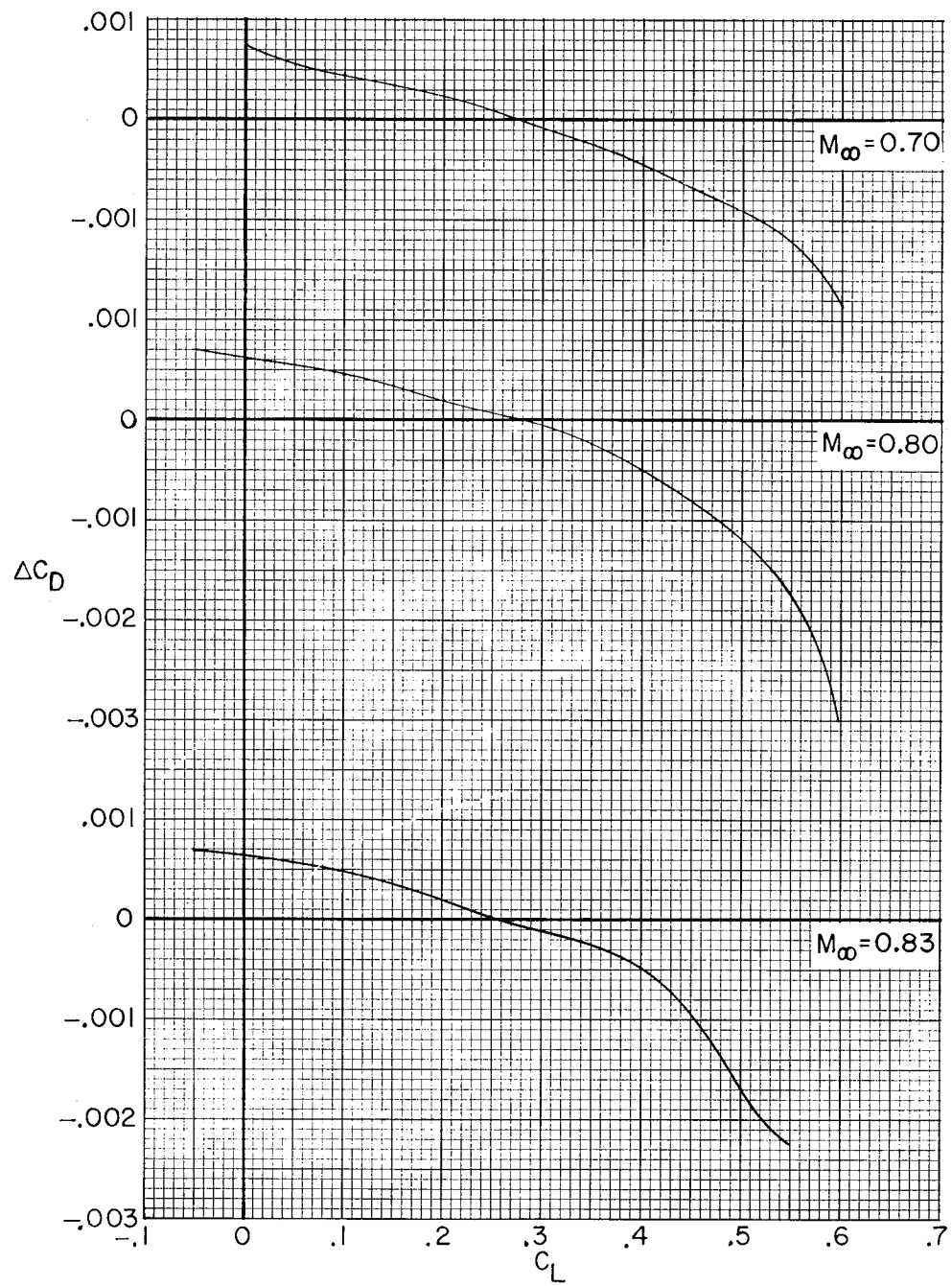
Figure 5.- Variations of incremental drag coefficient with lift coefficient;

$$\Delta C_D = \left(C_D\right)_{\text{winglets on}} - \left(C_D\right)_{\text{basic tip}}.$$
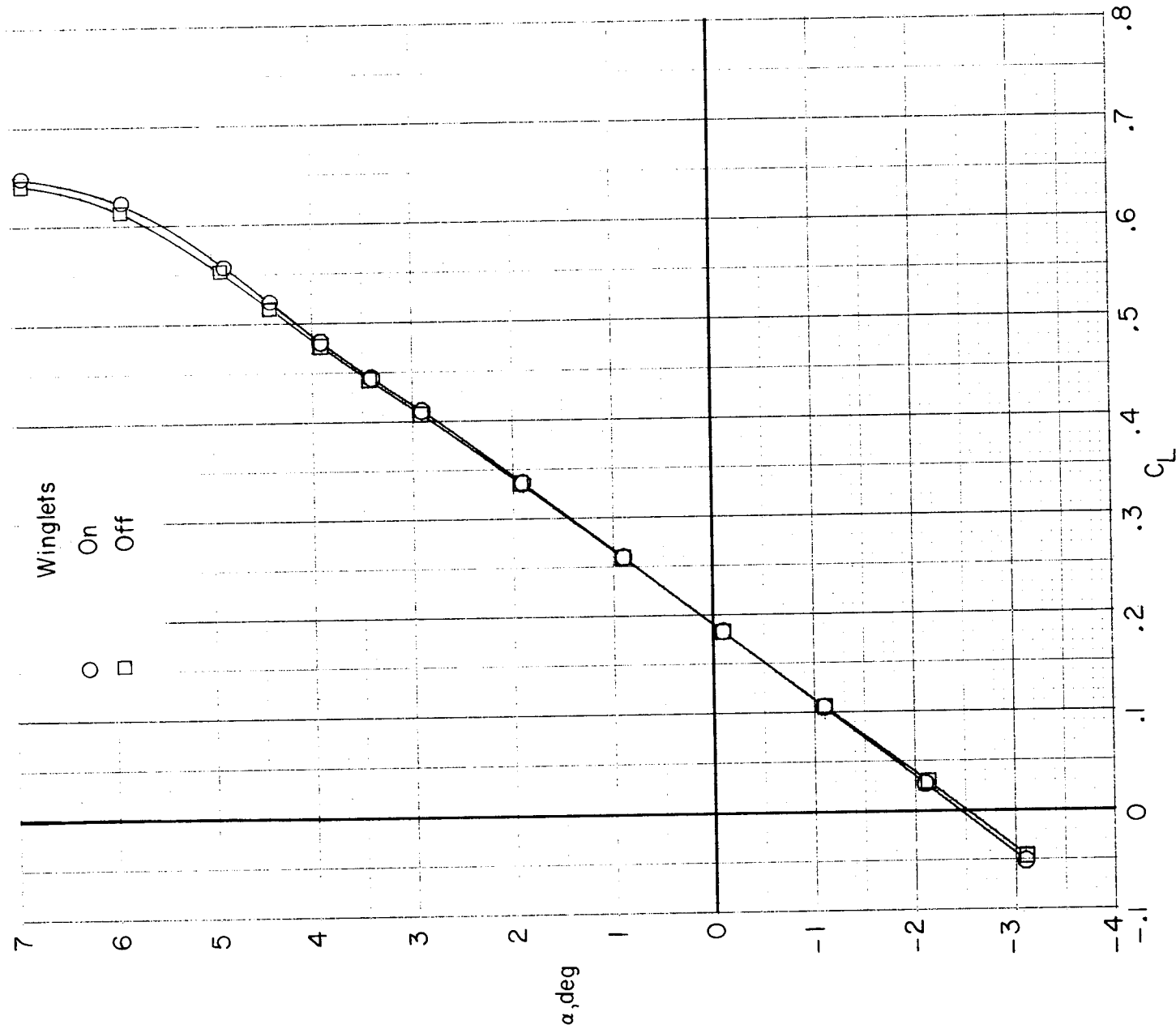
(a) $M_\infty = 0.700$.

Figure 6.- Variation of angle of attack with lift coefficient.

23
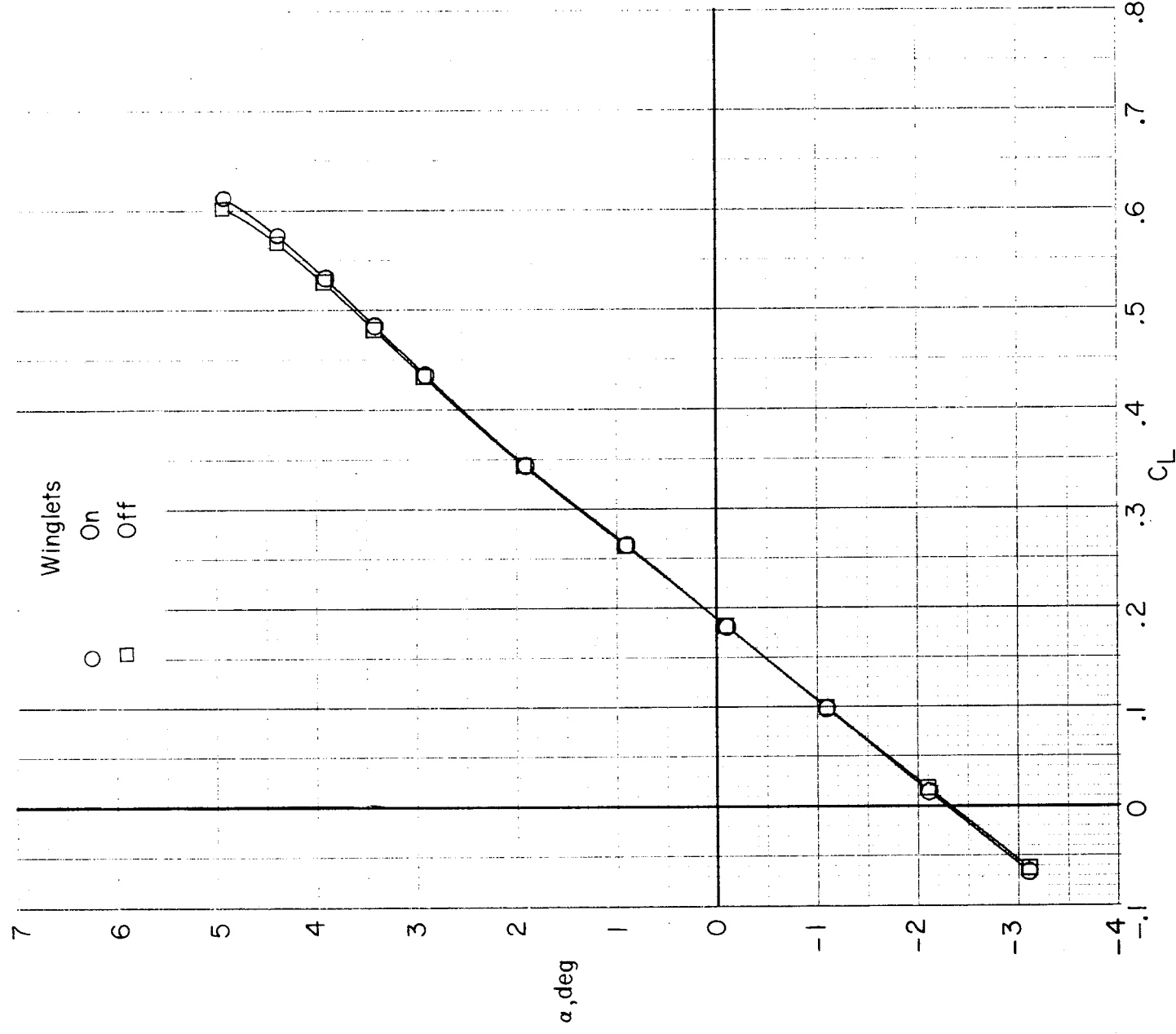
(b) $M_\infty = 0.800.$

Figure 6.- Continued.
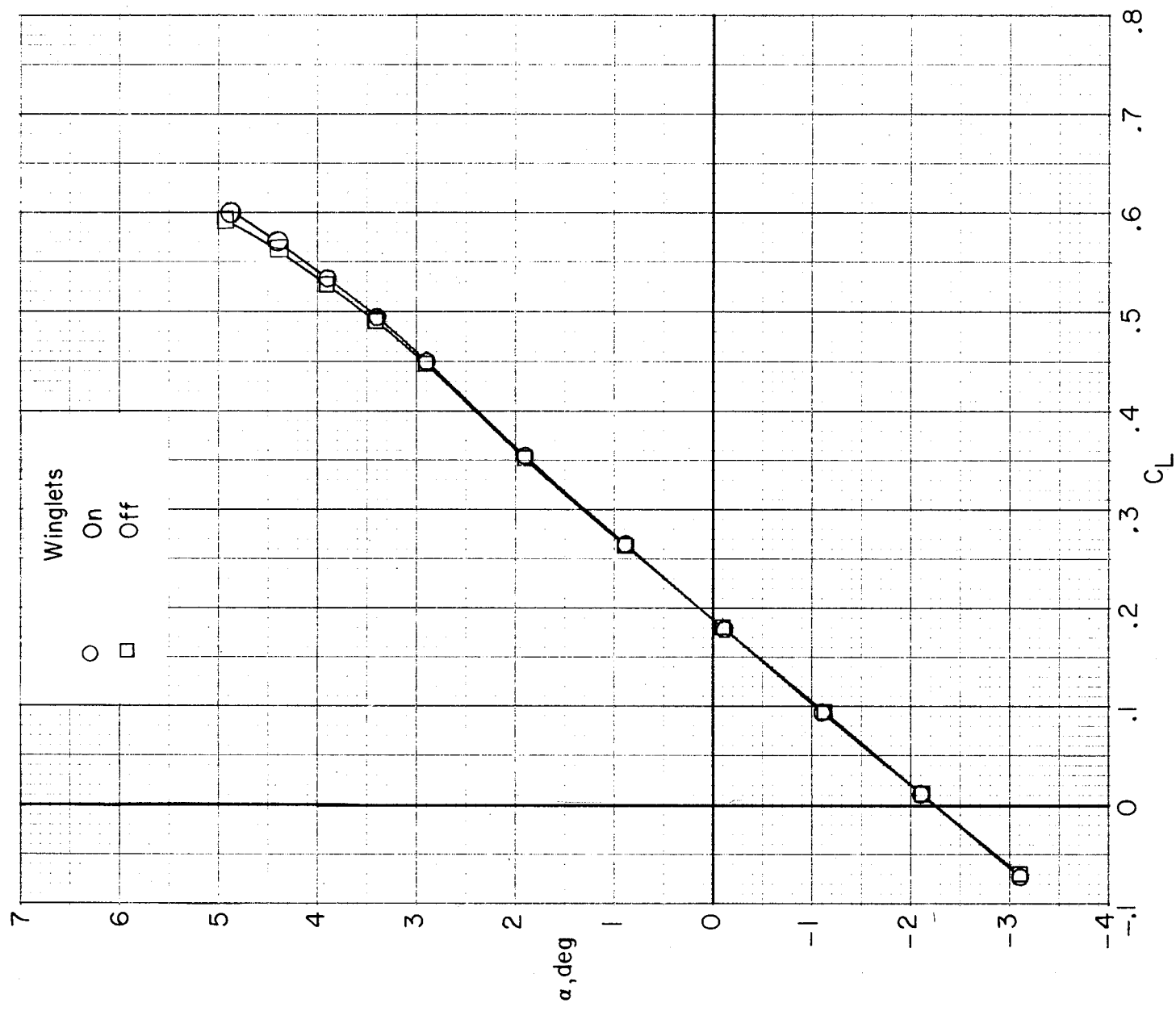
(c) $M_\infty = 0.830$.

Figure 6.- Concluded.

25
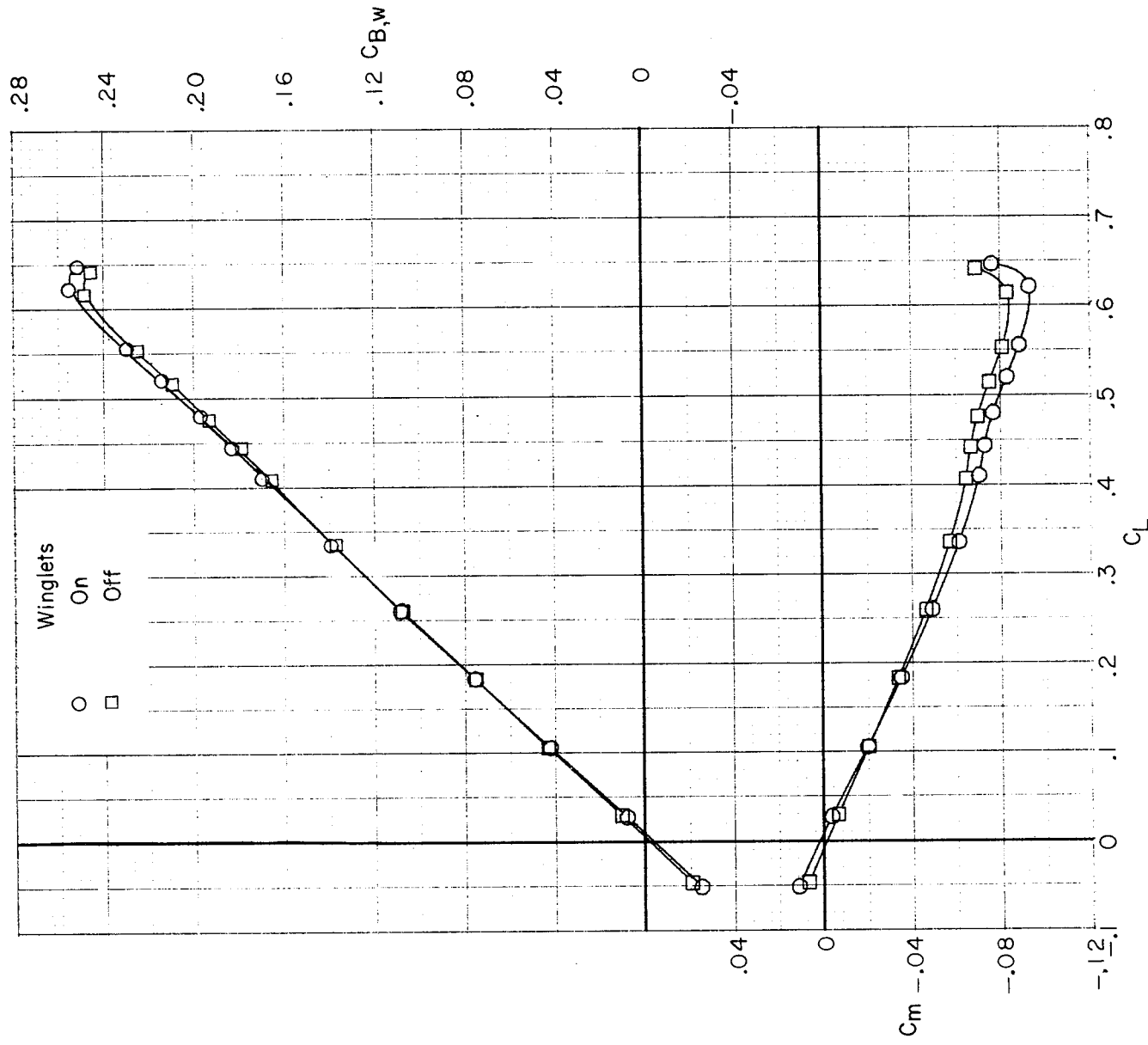
Figure 7.- Variation of wing-root bending-moment coefficient and pitching-moment coefficient with lift coefficient.

(a) $M_\infty = 0.700$.

26
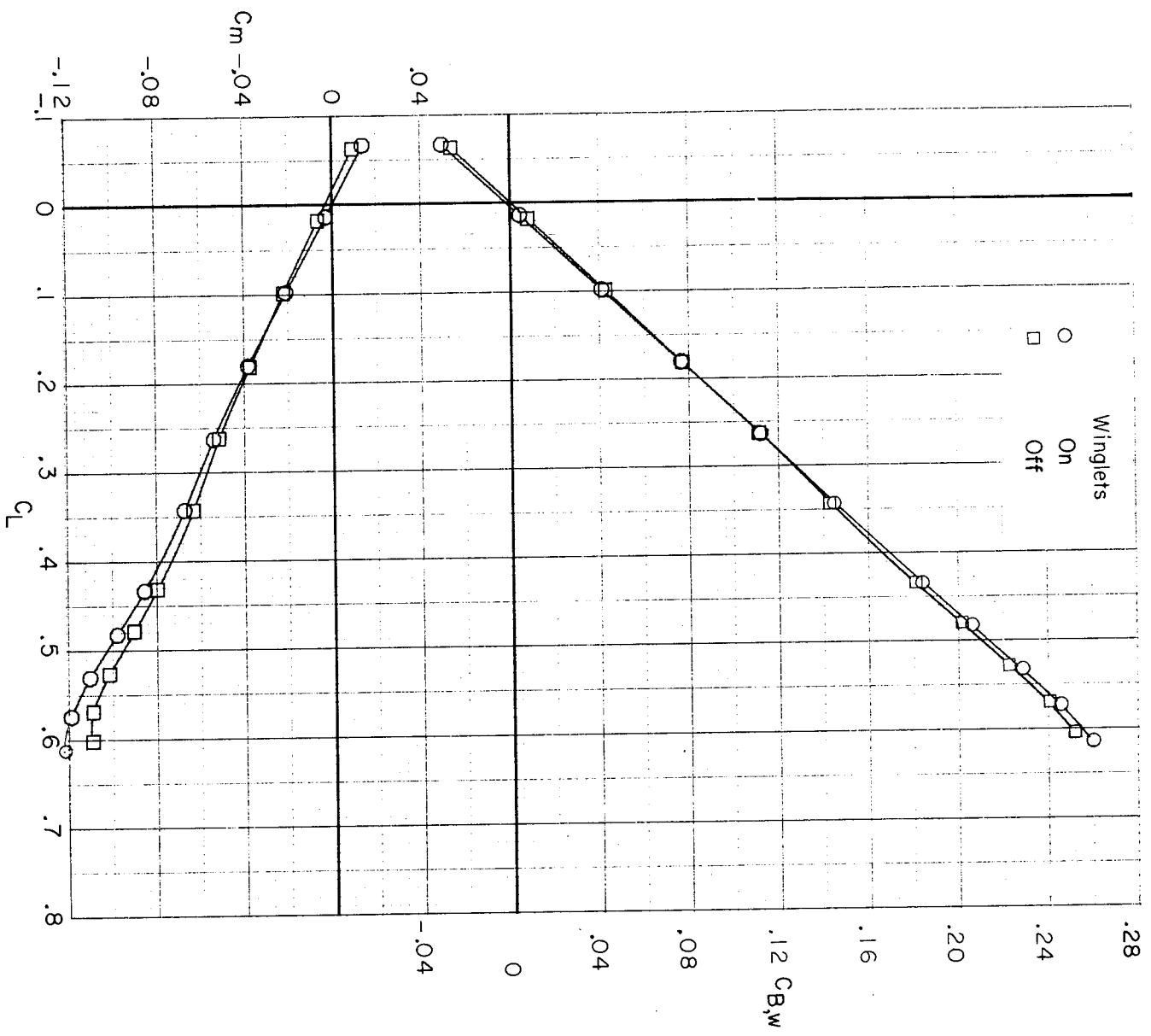
(b) $M_\infty = 0.800$.

Figure 7.- Continued.
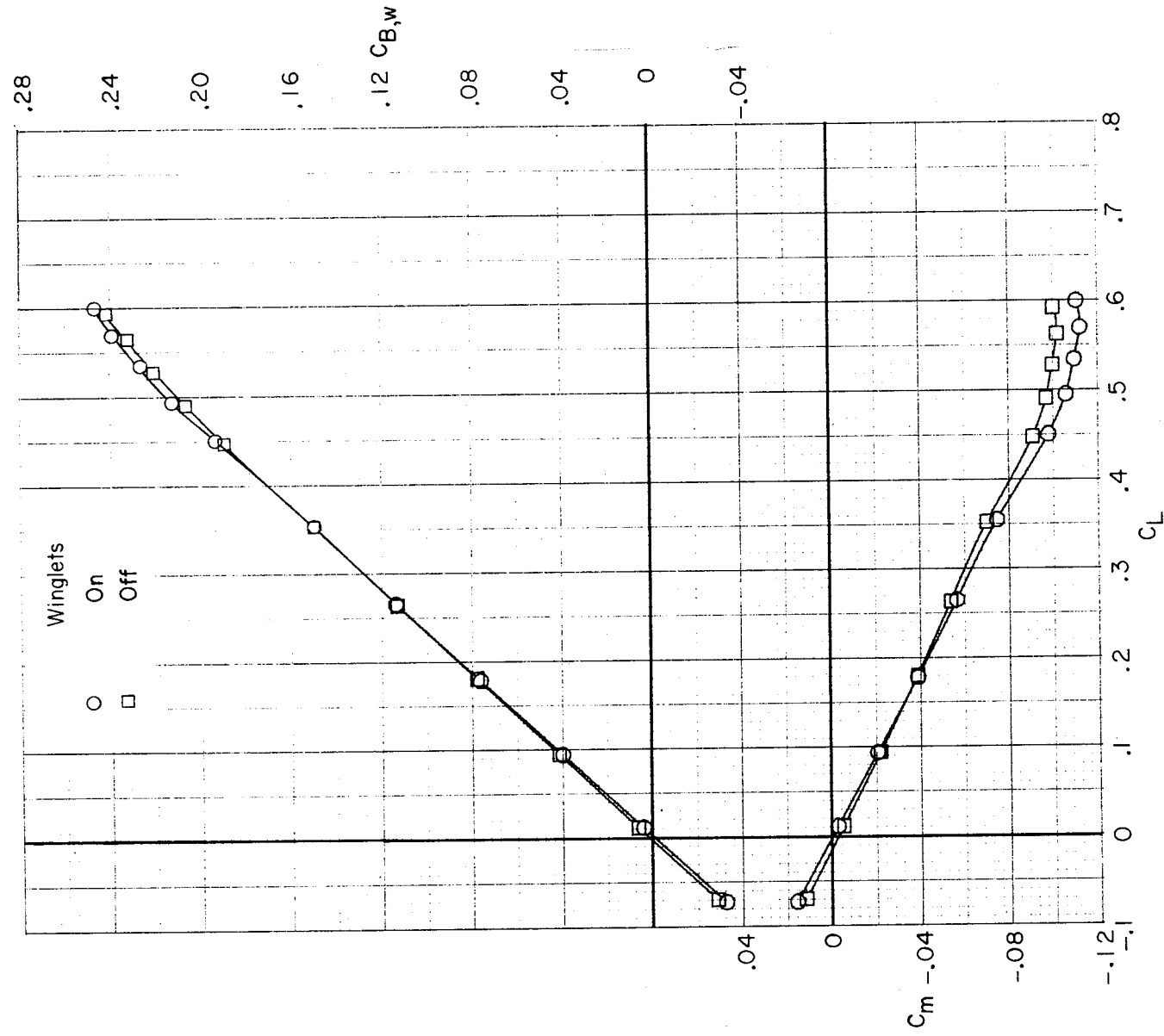
(c) $M_\infty = 0.830$.

Figure 7.- Concluded.
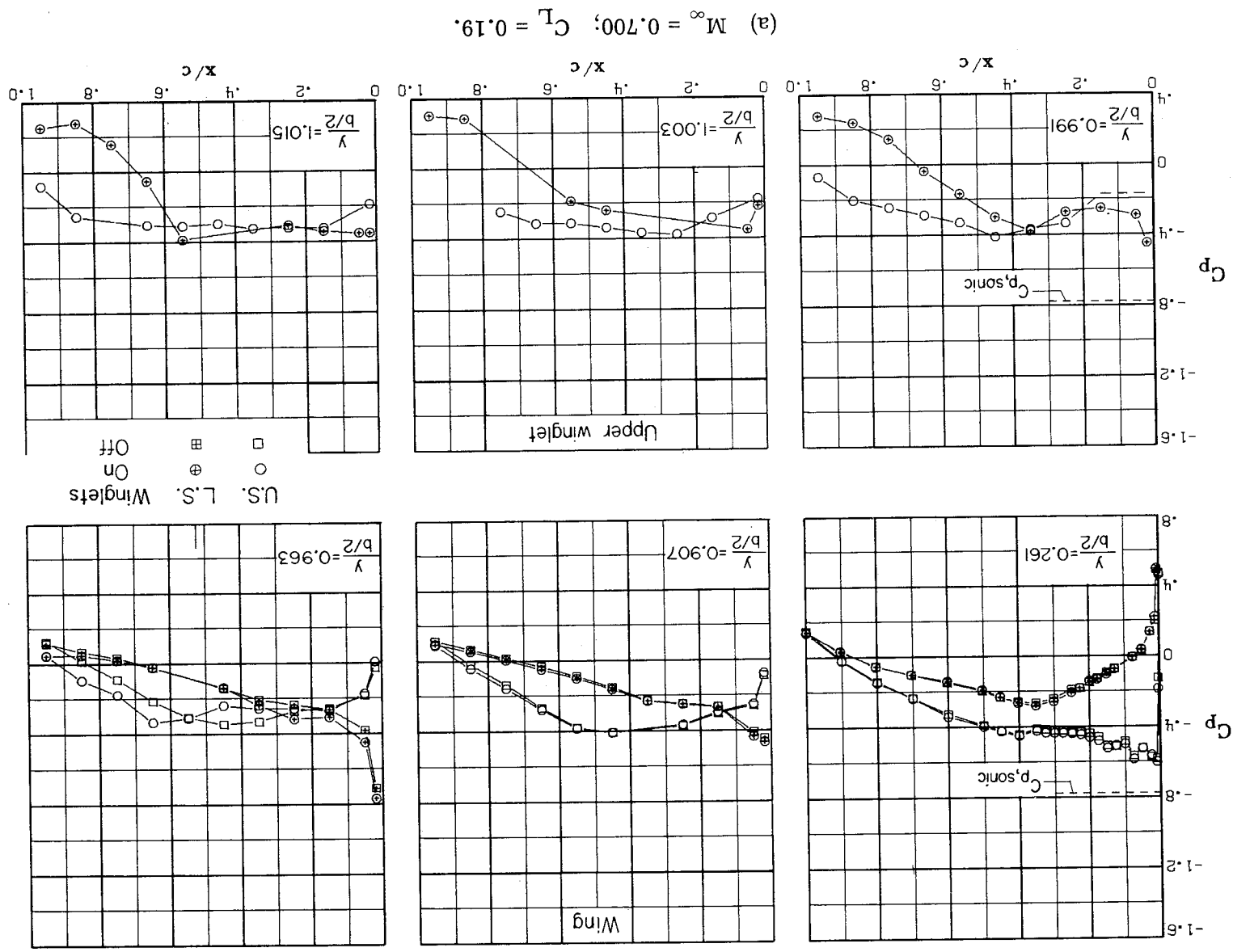
Figure 8.- Chordwise pressure distributions on wing and upper winglet.
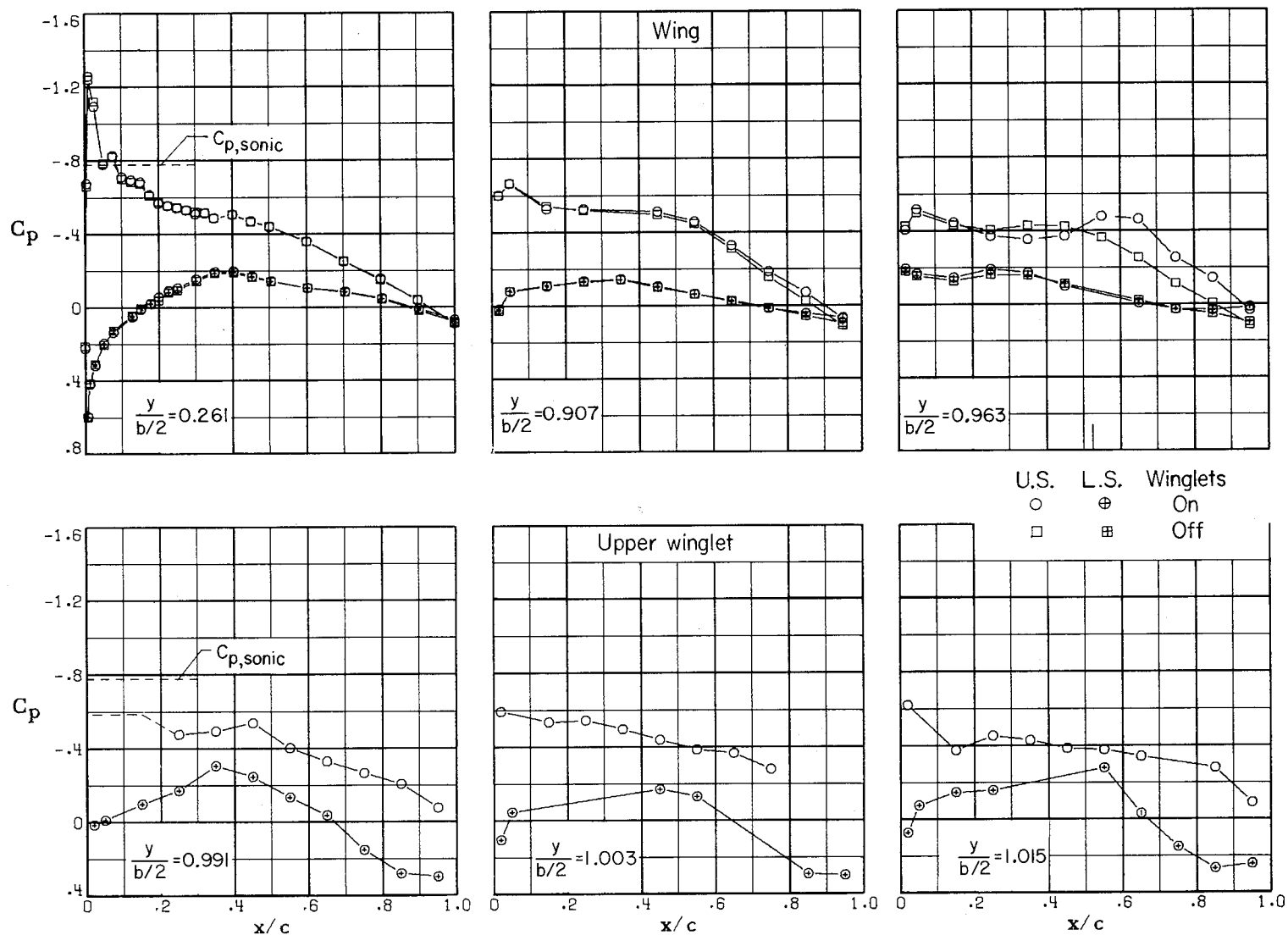
(a) $M_\infty = 0.700$; $C_L = 0.19$.

(b) $M_\infty = 0.700$; $C_L = 0.34$.

Figure 8.- Continued.
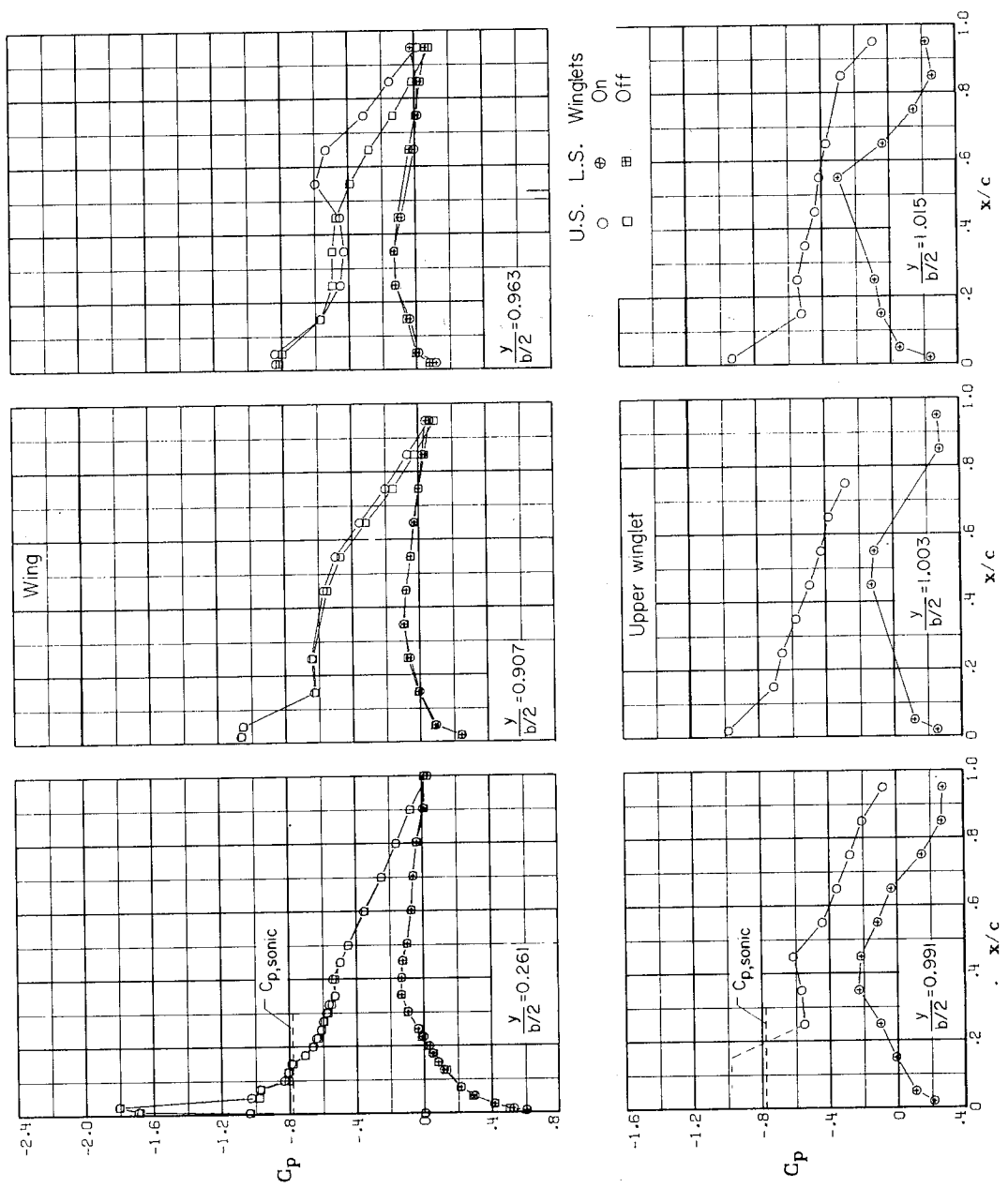
(c) $M_\infty = 0.700$; $C_L = 0.45$.

Figure 8.- Continued.

31

(d) $M_\infty = 0.700$; $C_L = 0.53$.
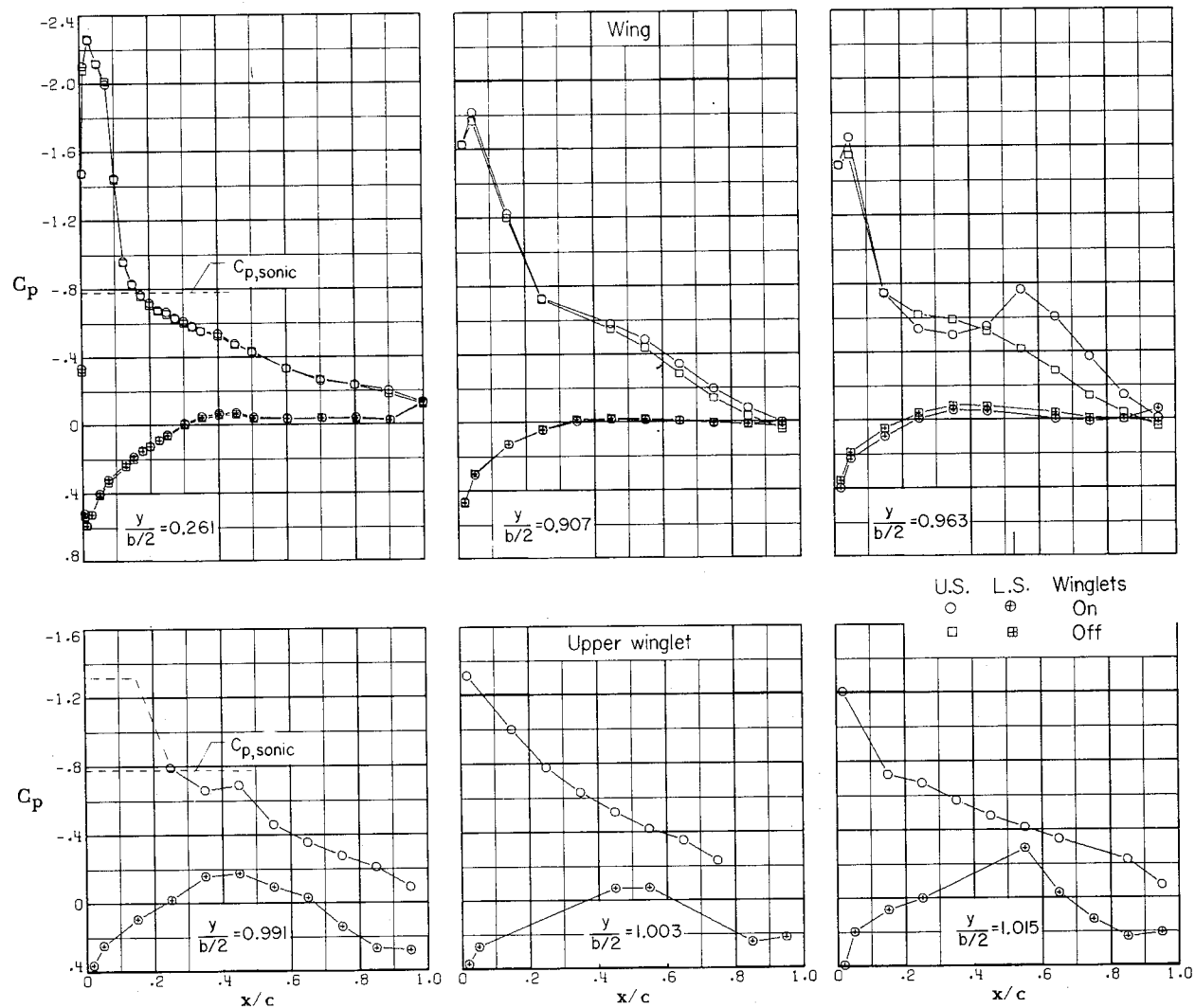
Figure 8.- Continued.

(e) $M_\infty = 0.700$; $C_L = 0.63$.

Figure 8.- Continued.
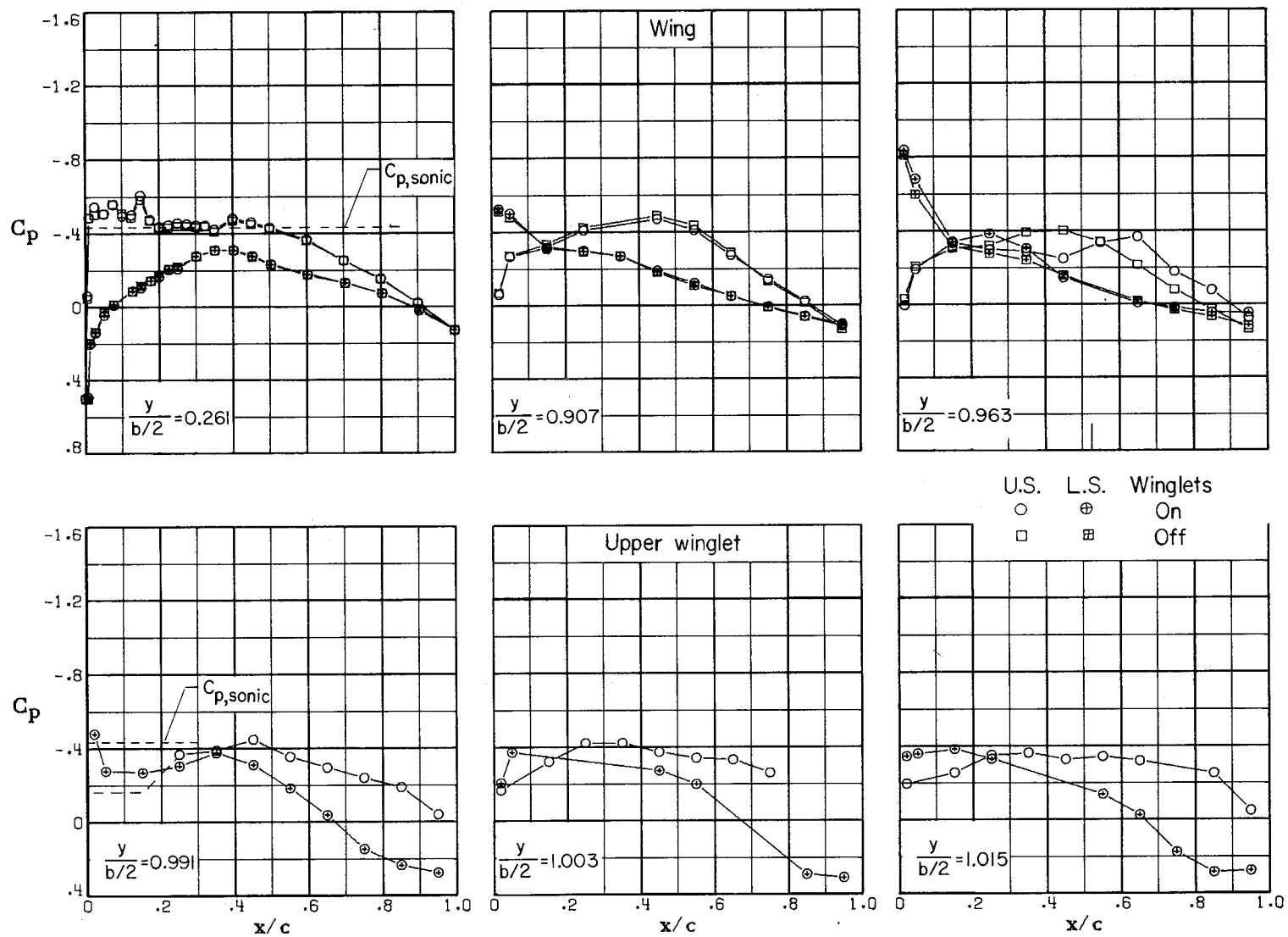
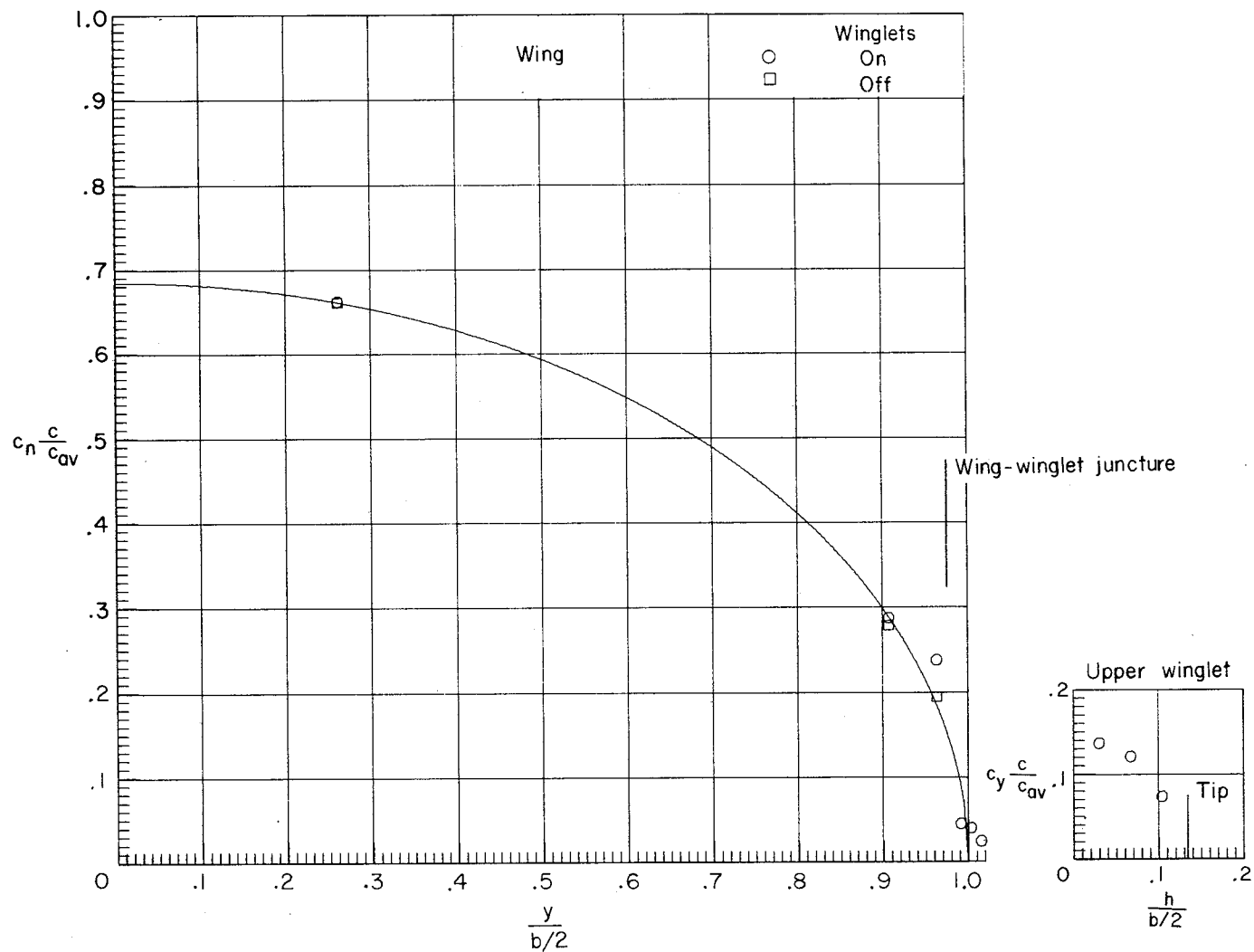(f) $M_\infty = 0.800$; $C_L = 0.18$.

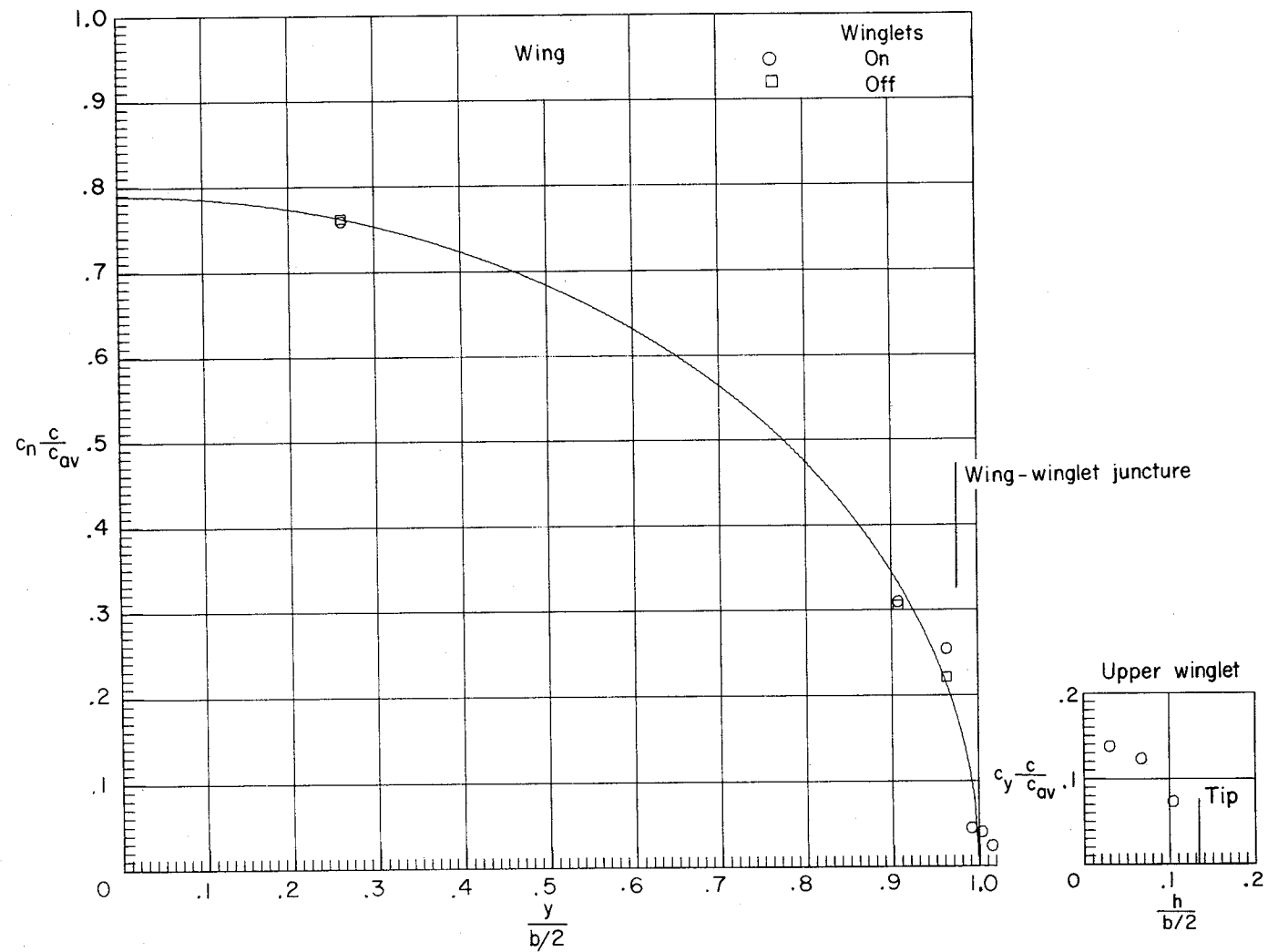Figure 8.- Continued.

(h) $M_\infty = 0.800$; $C_L = 0.44$.

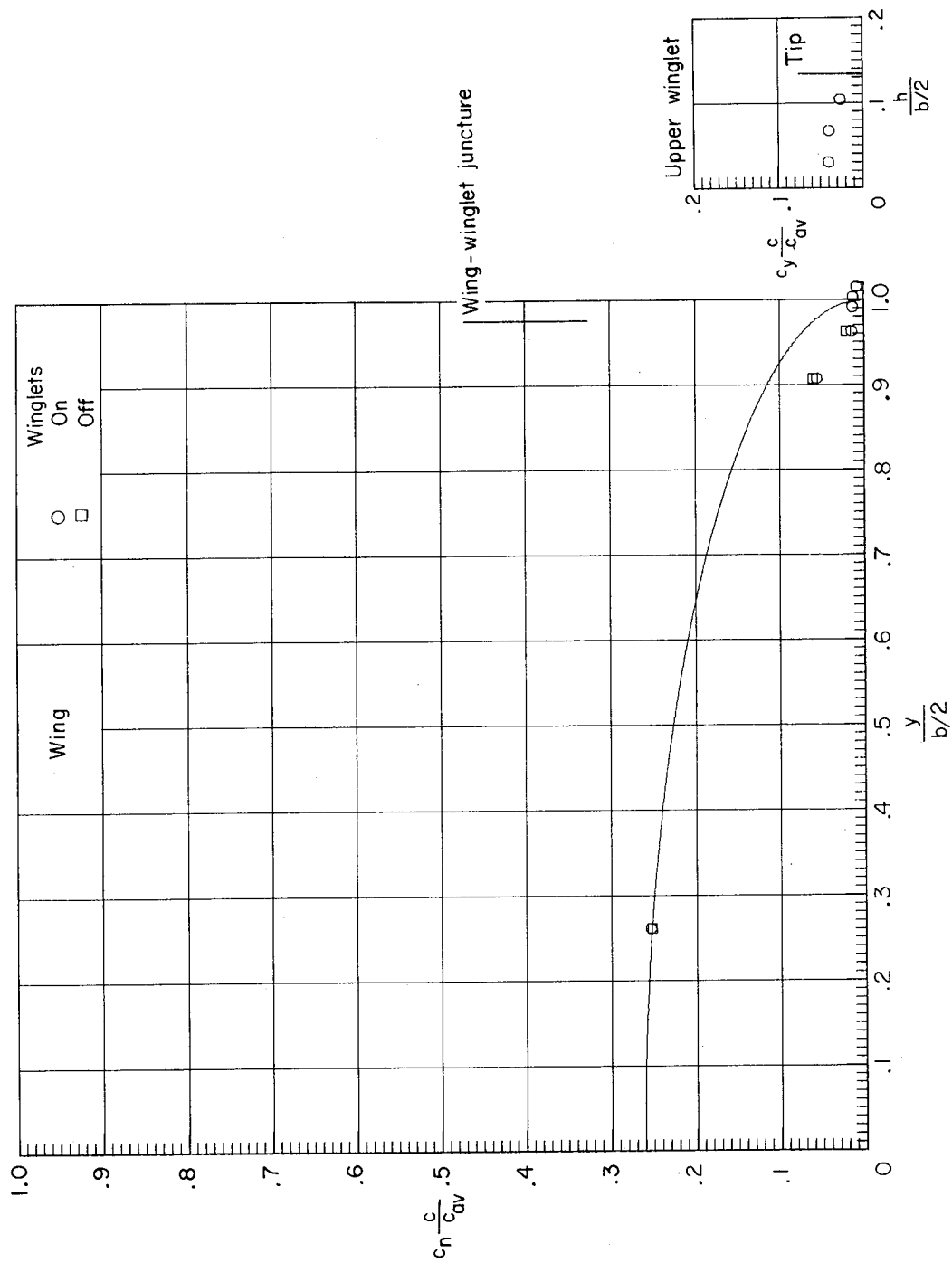Figure 8.- Continued.

(i) $M_\infty = 0.800$; $C_L = 0.54$.

Figure 8.- Continued.
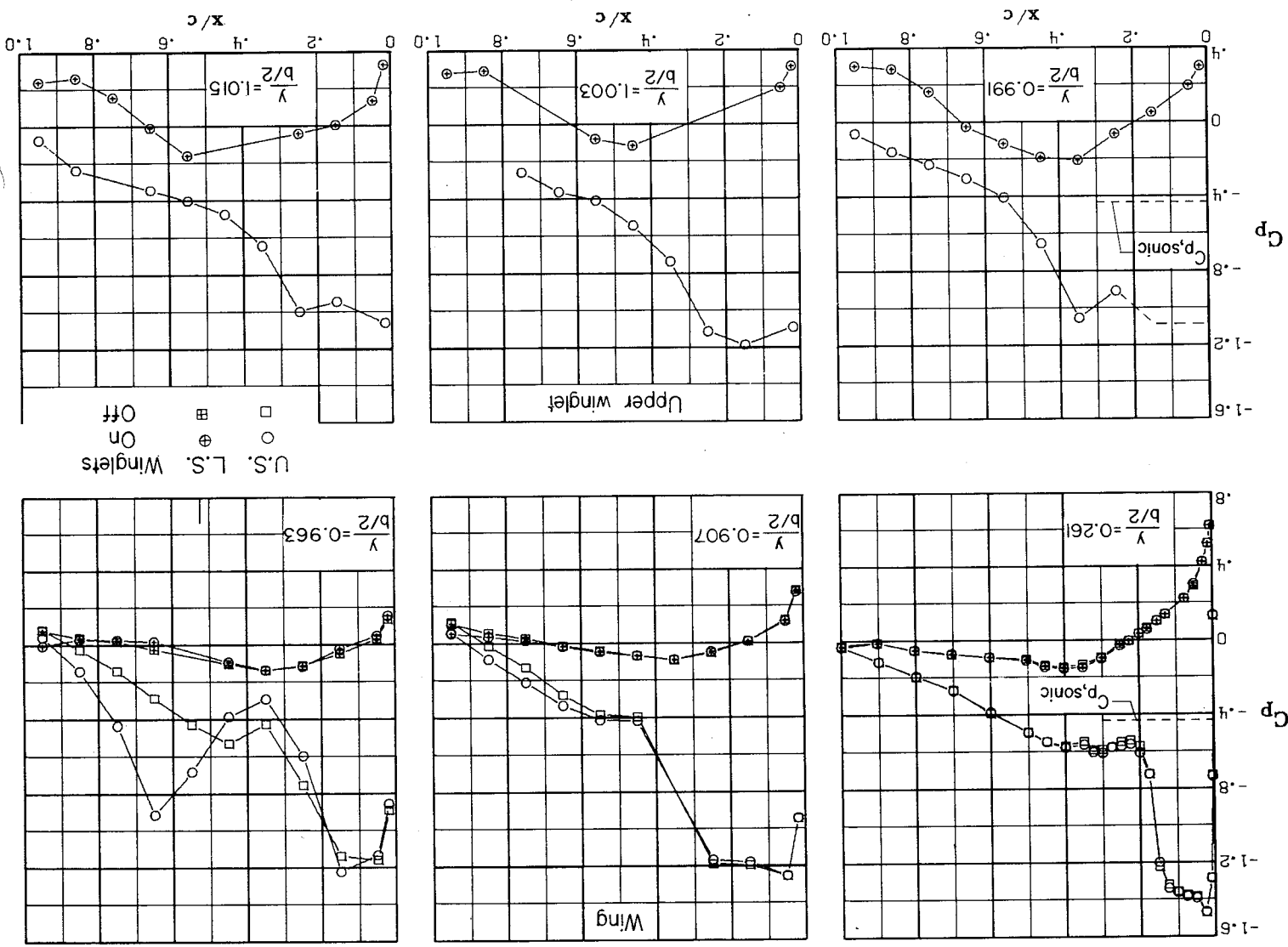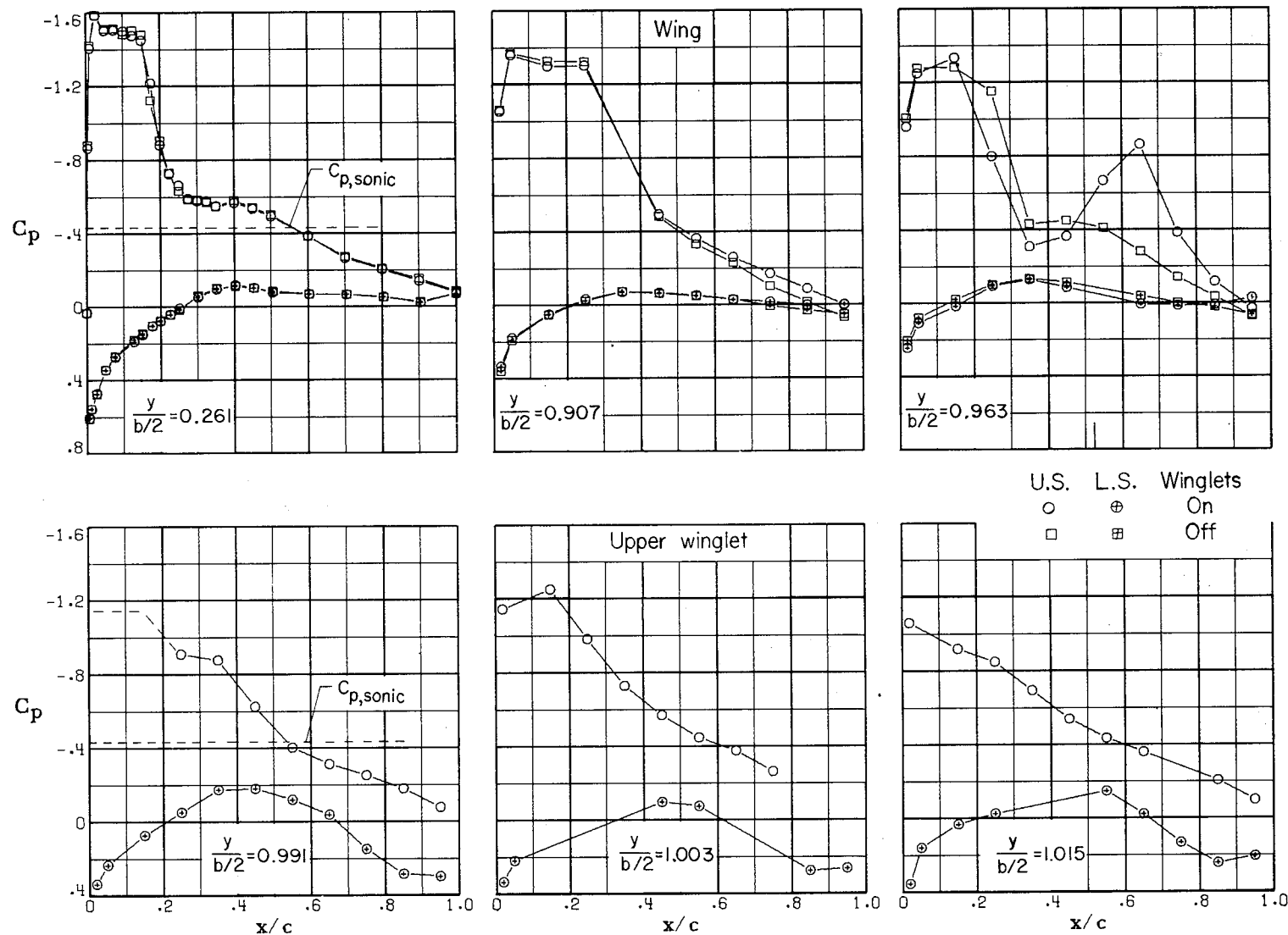
(j) $M_\infty = 0.800$; $C_L = 0.61$.

Figure 8.- Continued.
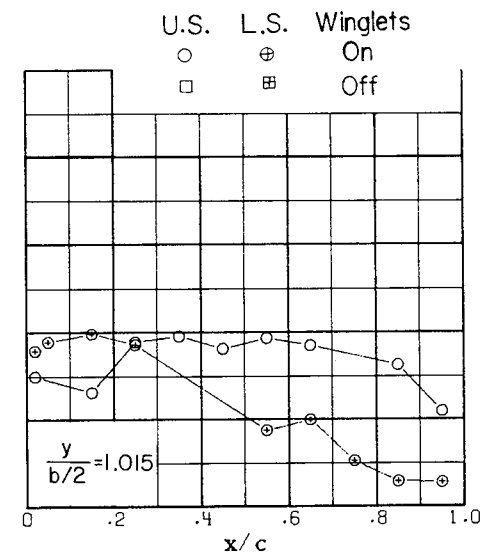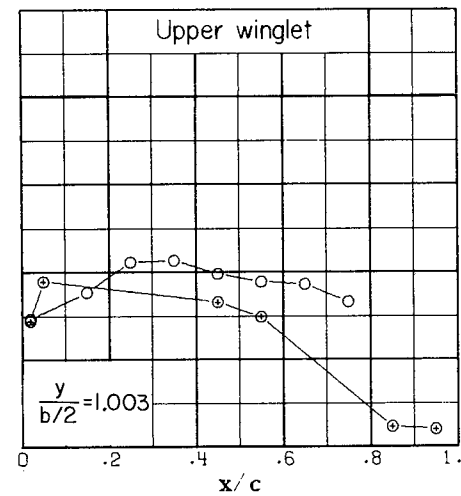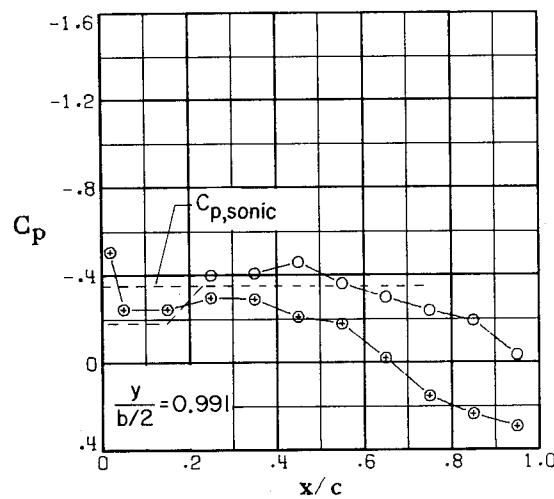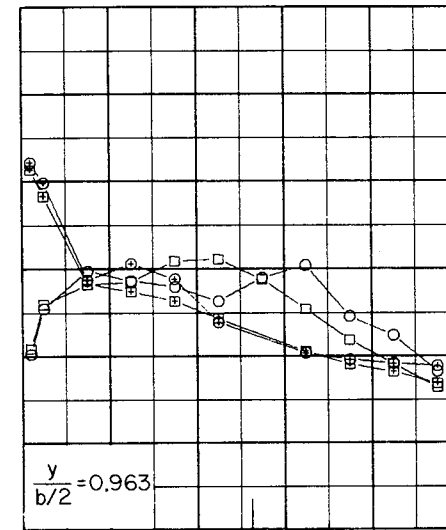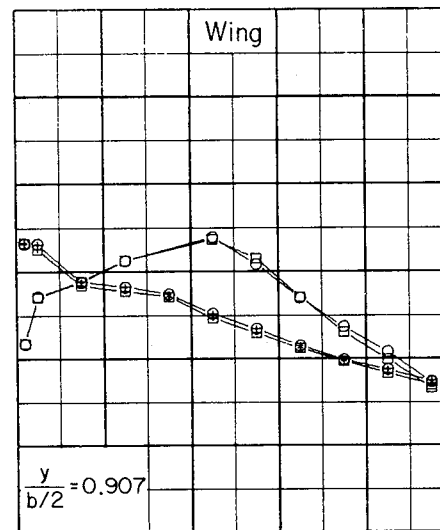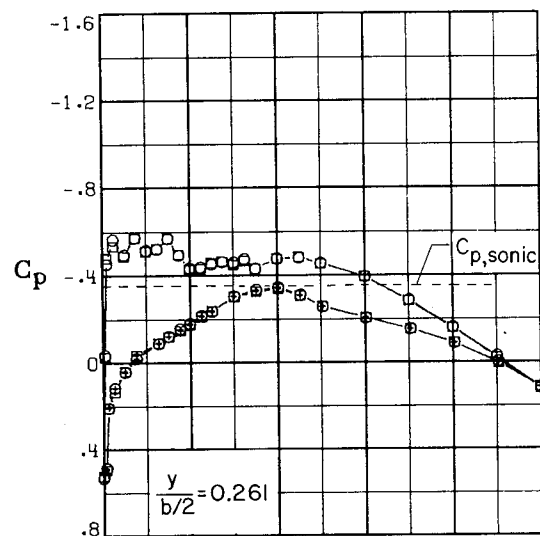
(k) $M_\infty = 0.830$; $C_L = 0.19$.

Figure 8.- Continued.
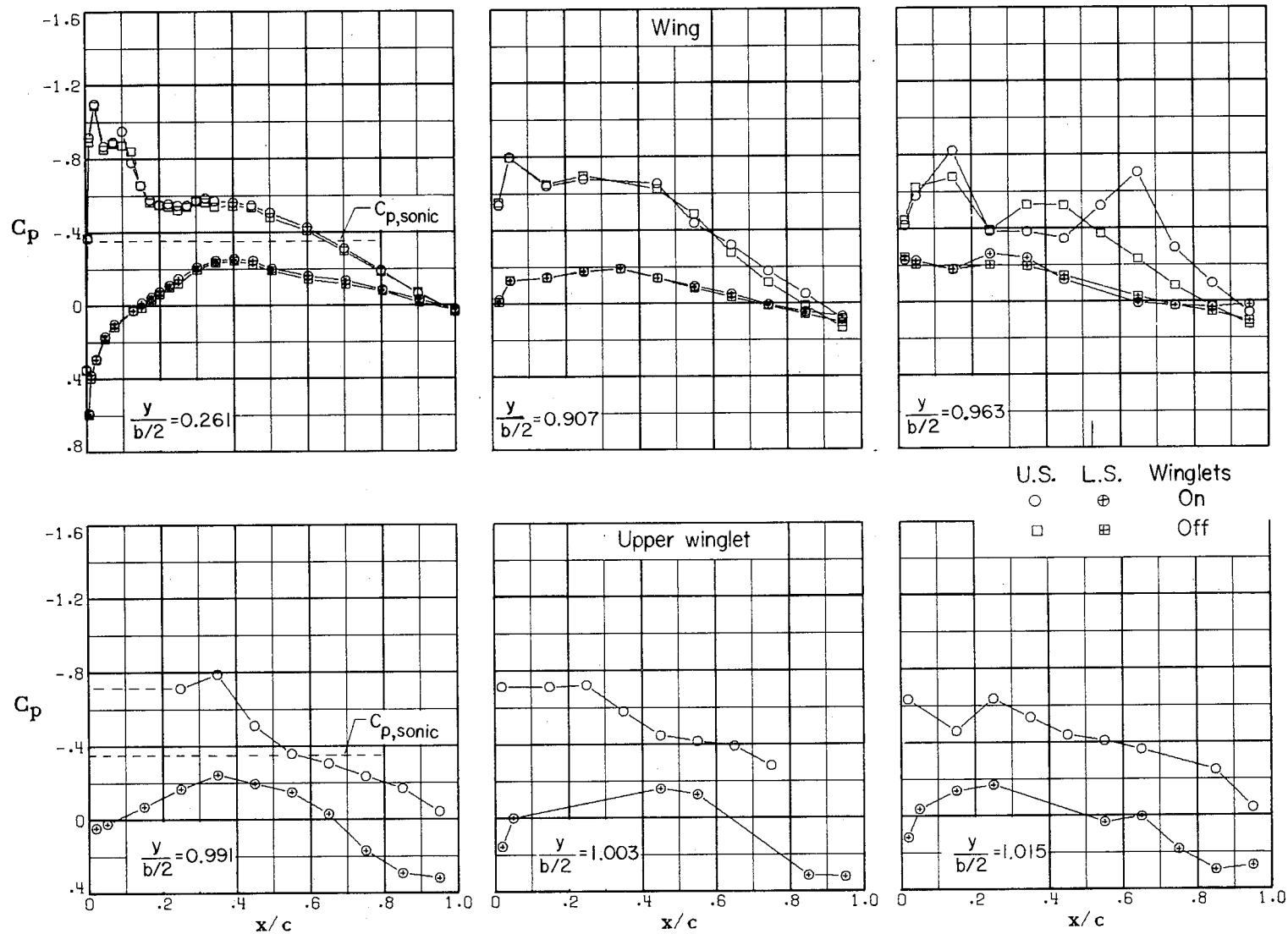
(1) $M_\infty = 0.830$; $C_L = 0.36$.

Figure 8.- Continued.

40
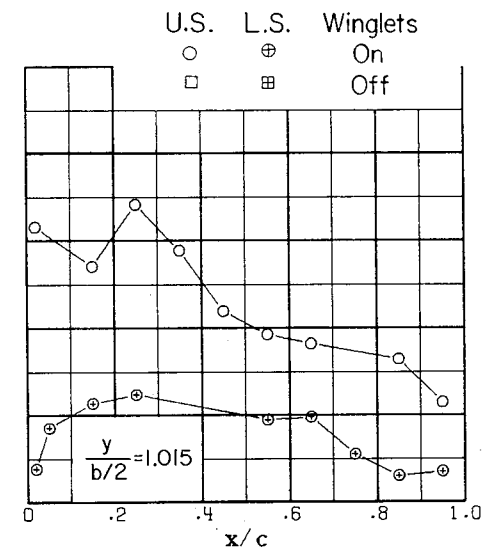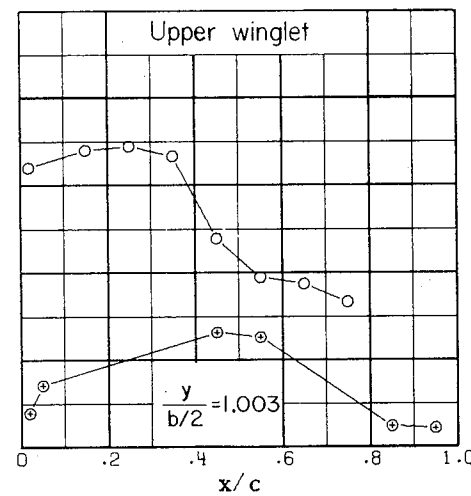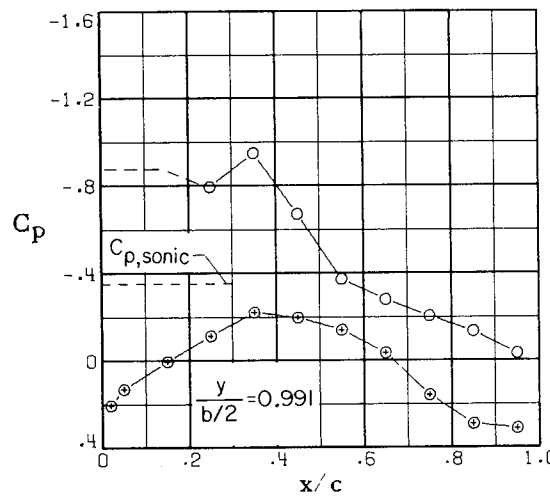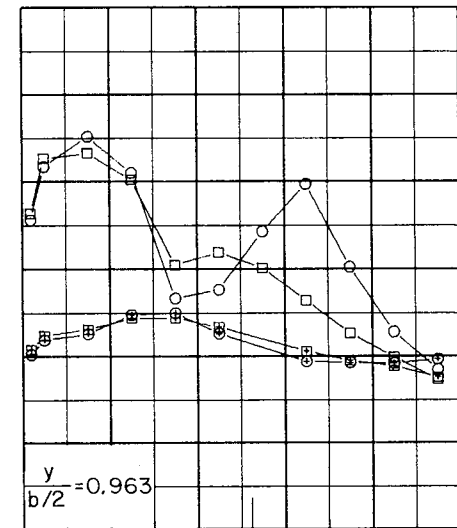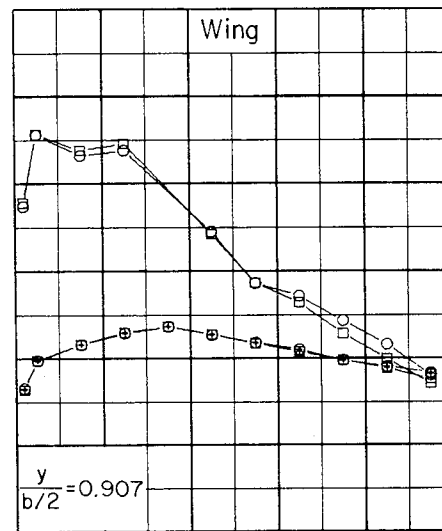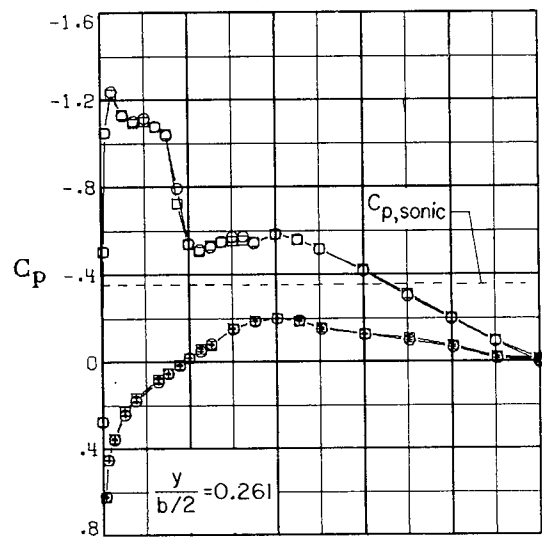
(m)　$M_\infty = 0.830;$　$C_L = 0.46.$

Figure 8.- Continued.
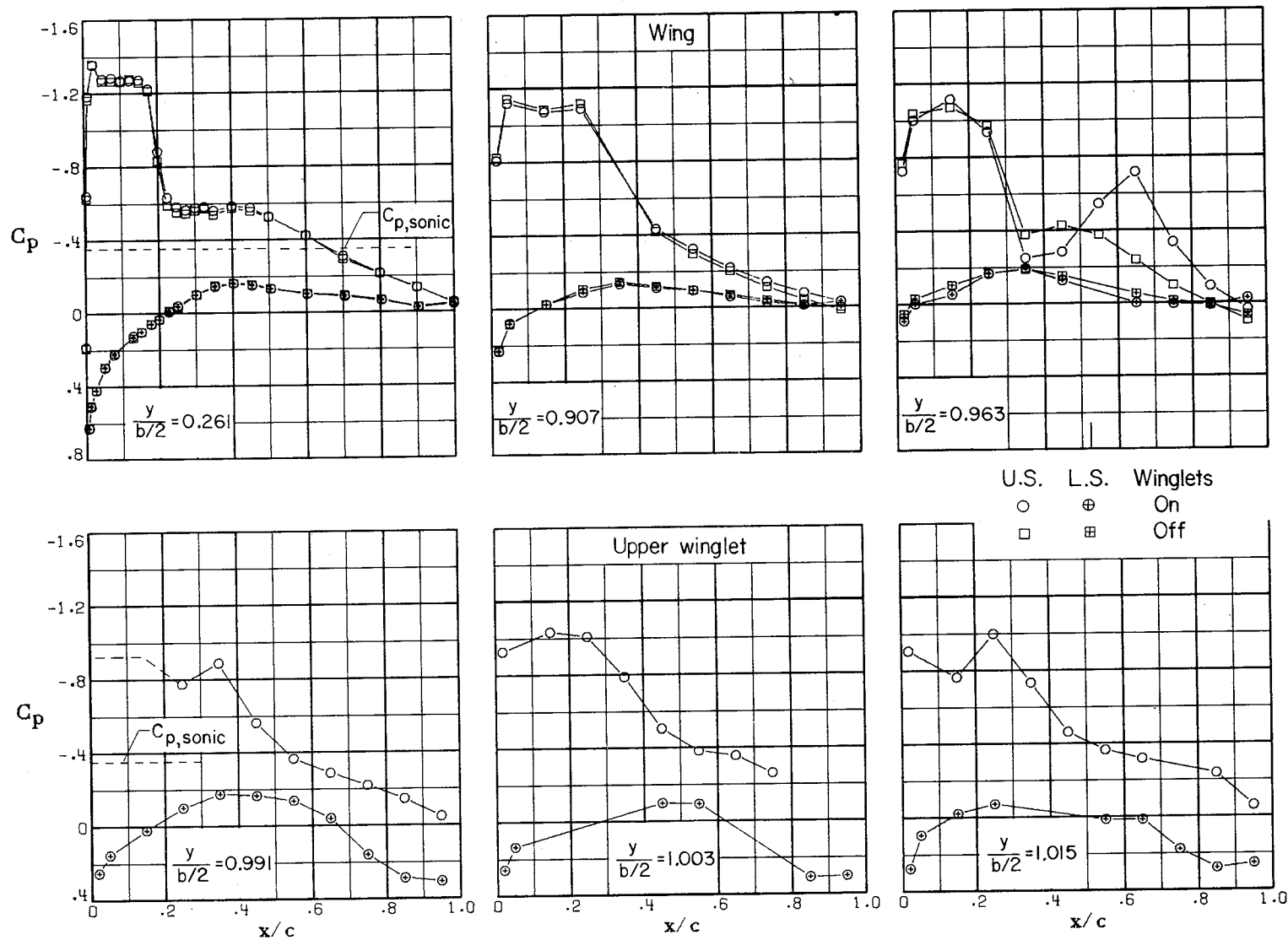
(n) $M_\infty = 0.830$; $C_L = 0.53$.

Figure 8.- Continued.

42
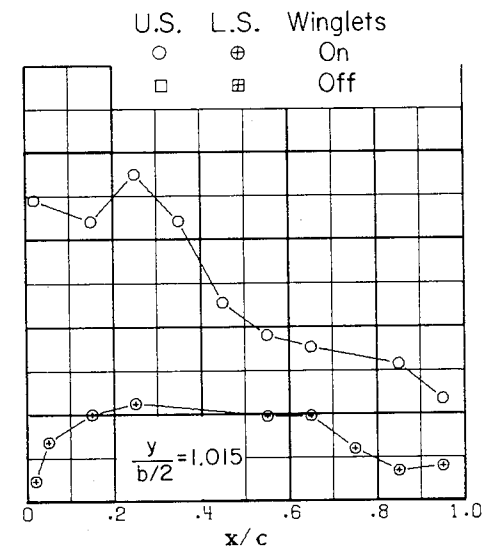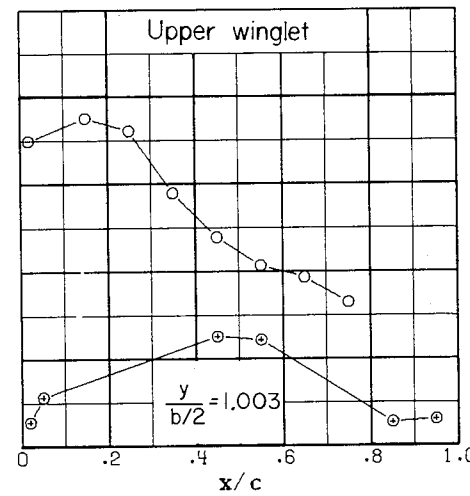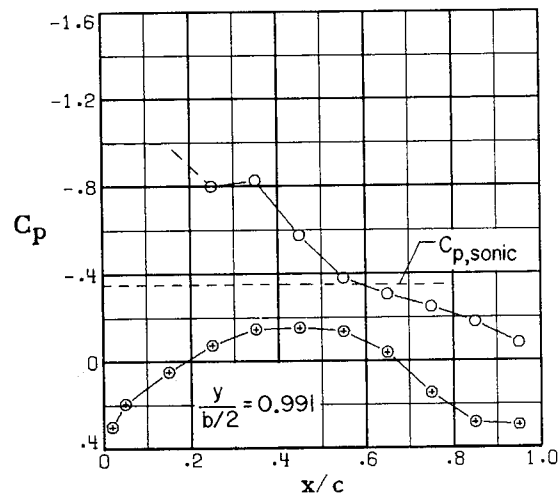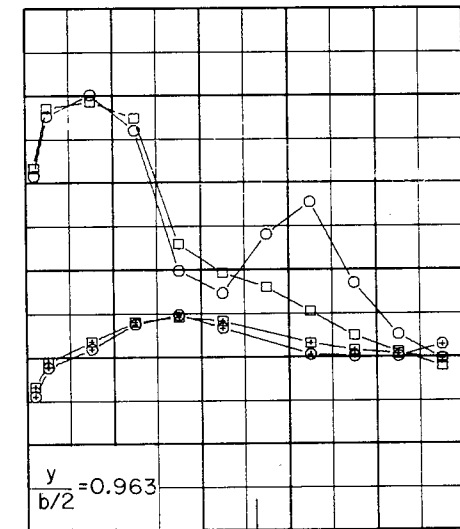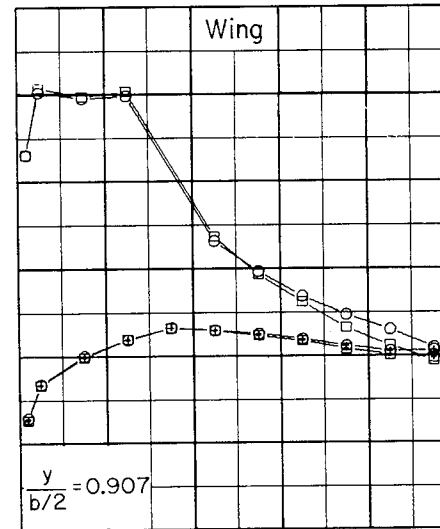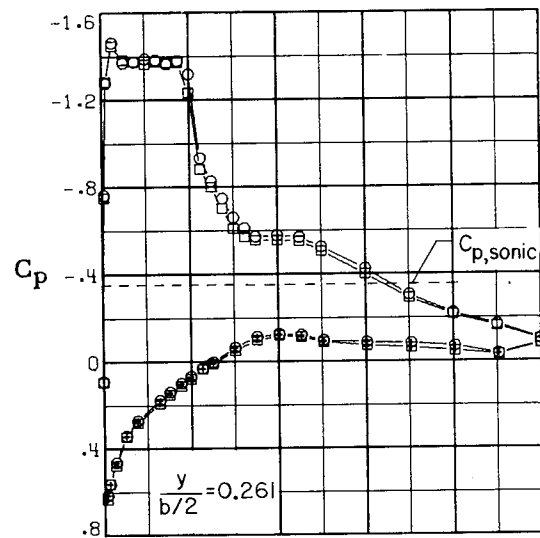
(o) $M_\infty = 0.830$; $C_L = 0.60$.

Figure 8.- Concluded.
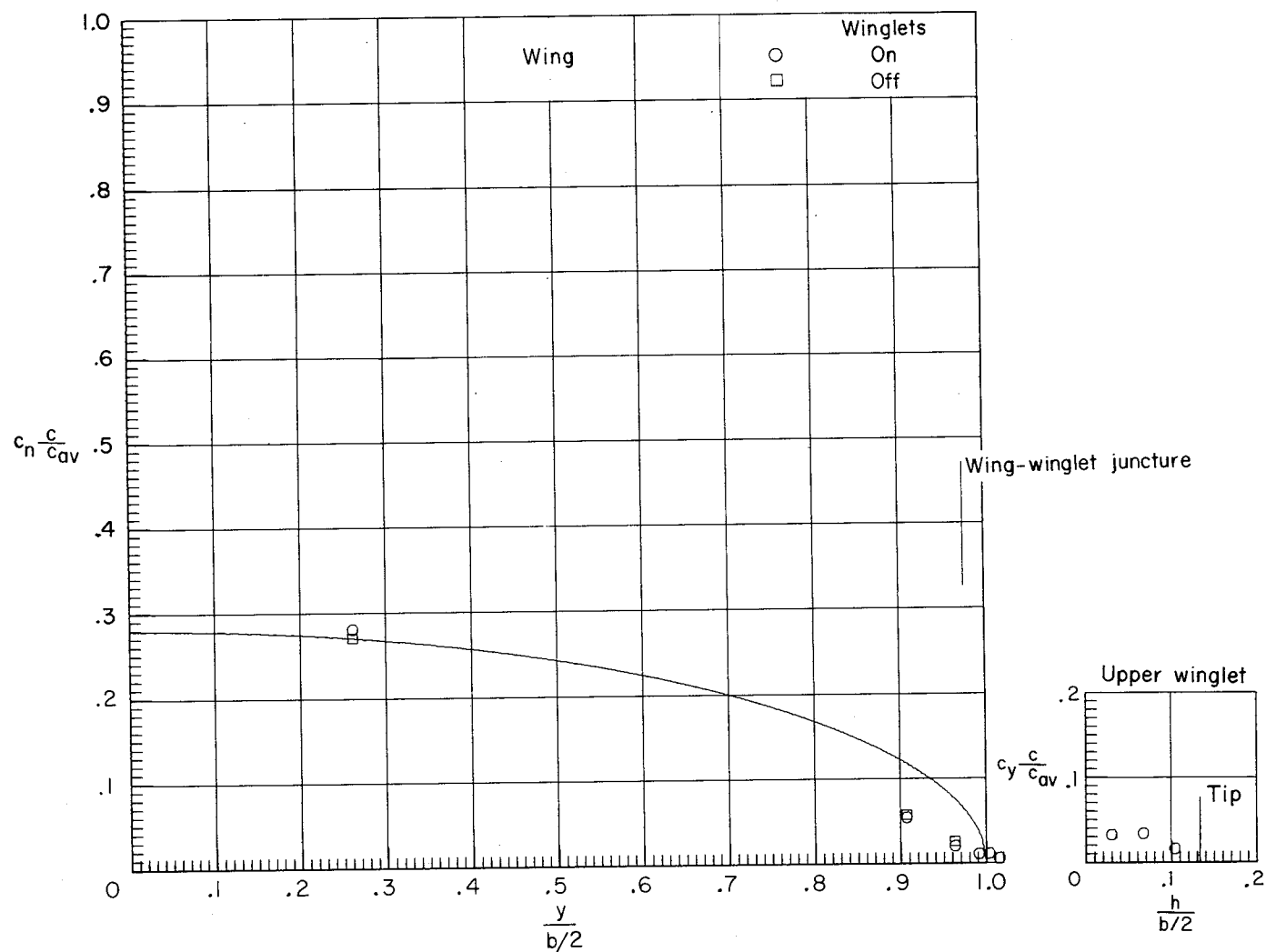
(a) $M_\infty = 0.700$; $C_L = 0.19$.

Figure 9.- Spanwise load distributions.   Elliptic load distribution for basic wing also shown.

(b) $M_\infty = 0.700$; $C_L = 0.34$.
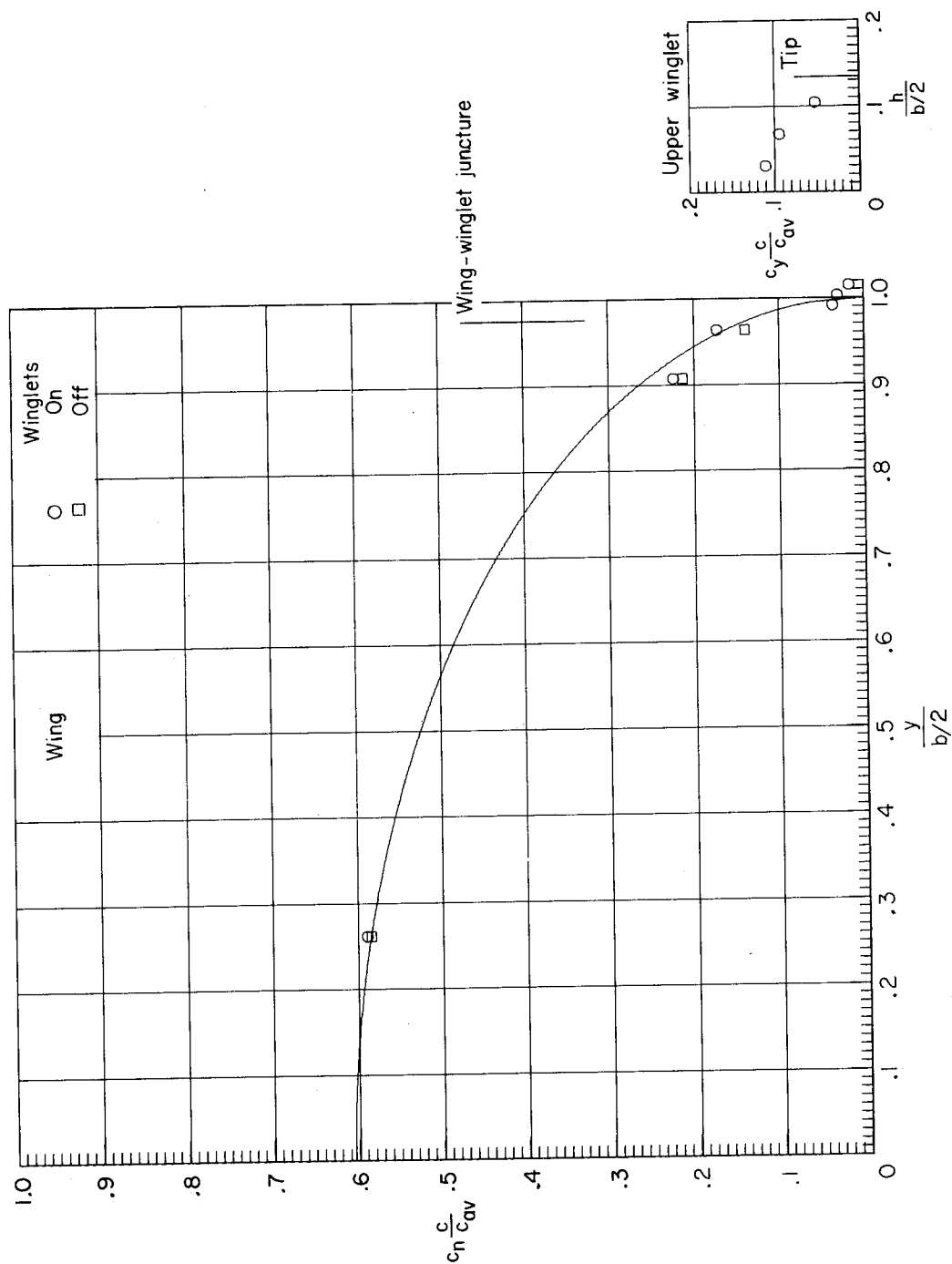
Figure 9.- Continued.

(c) $M_\infty = 0.700$; $C_L = 0.45$.

Figure 9.— Continued.
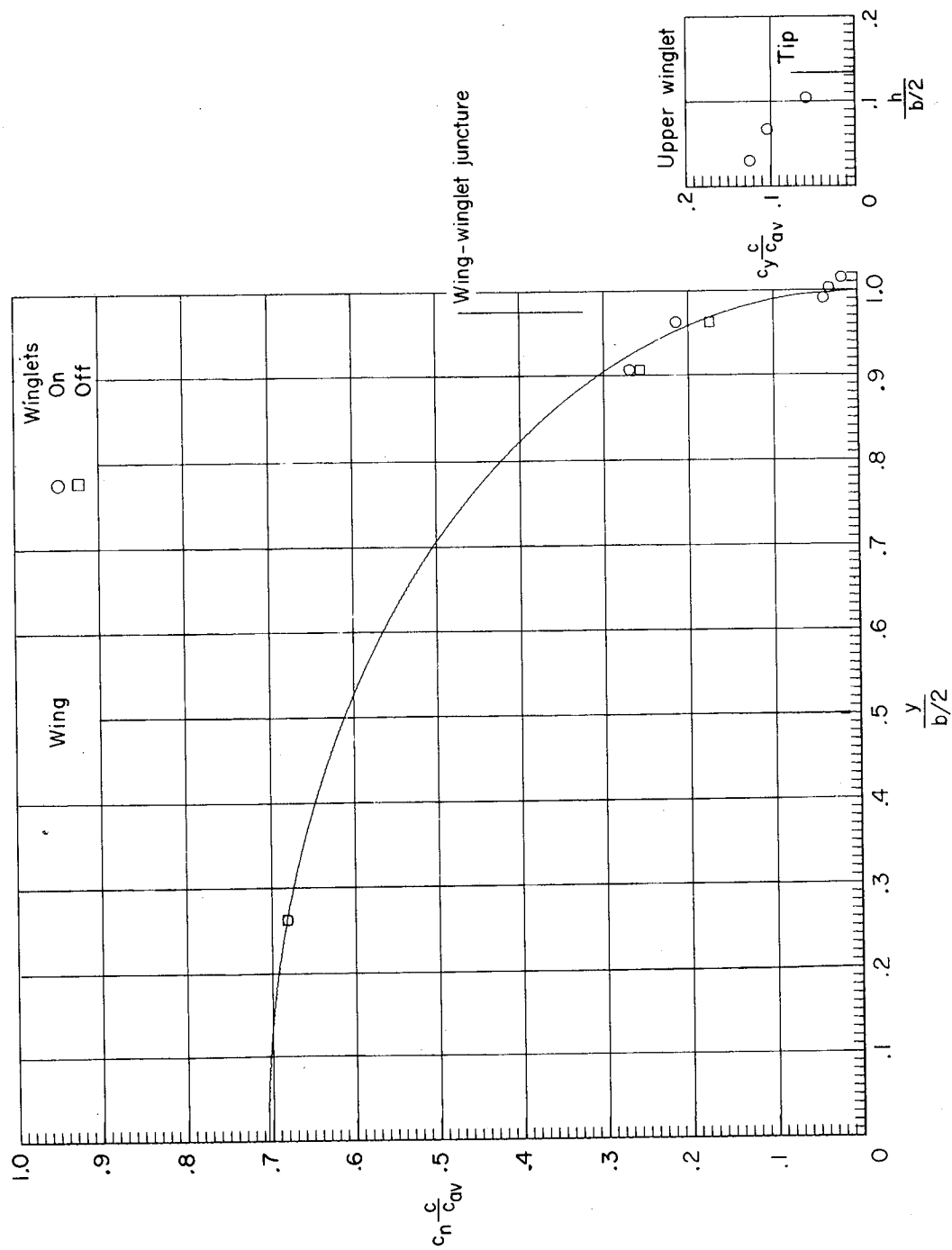
(d) $M_\infty = 0.700$; $C_L = 0.53$.

Figure 9.- Continued.

47
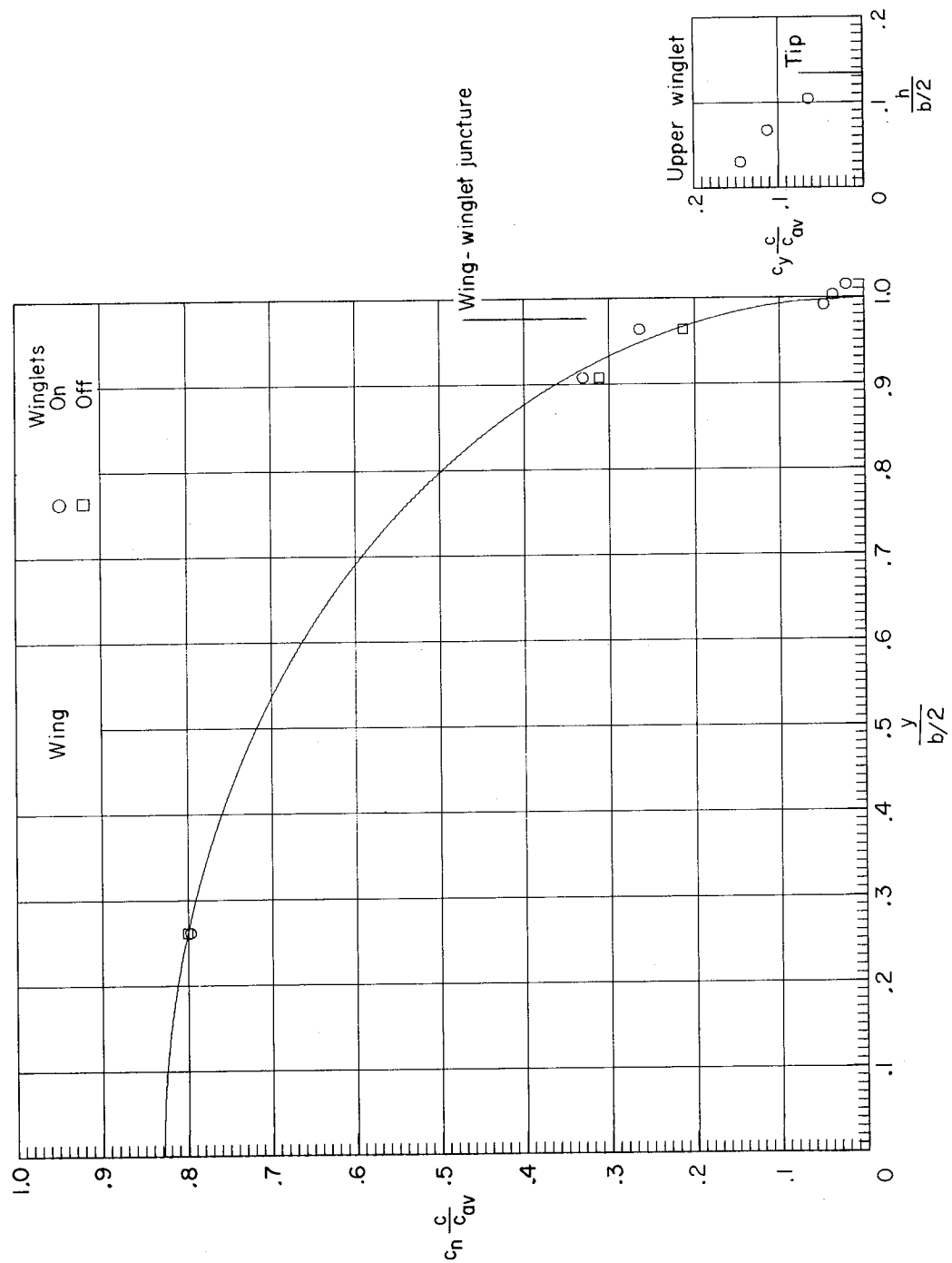
(e) $M_\infty = 0.700$; $C_L = 0.63$.

Figure 9.- Continued.
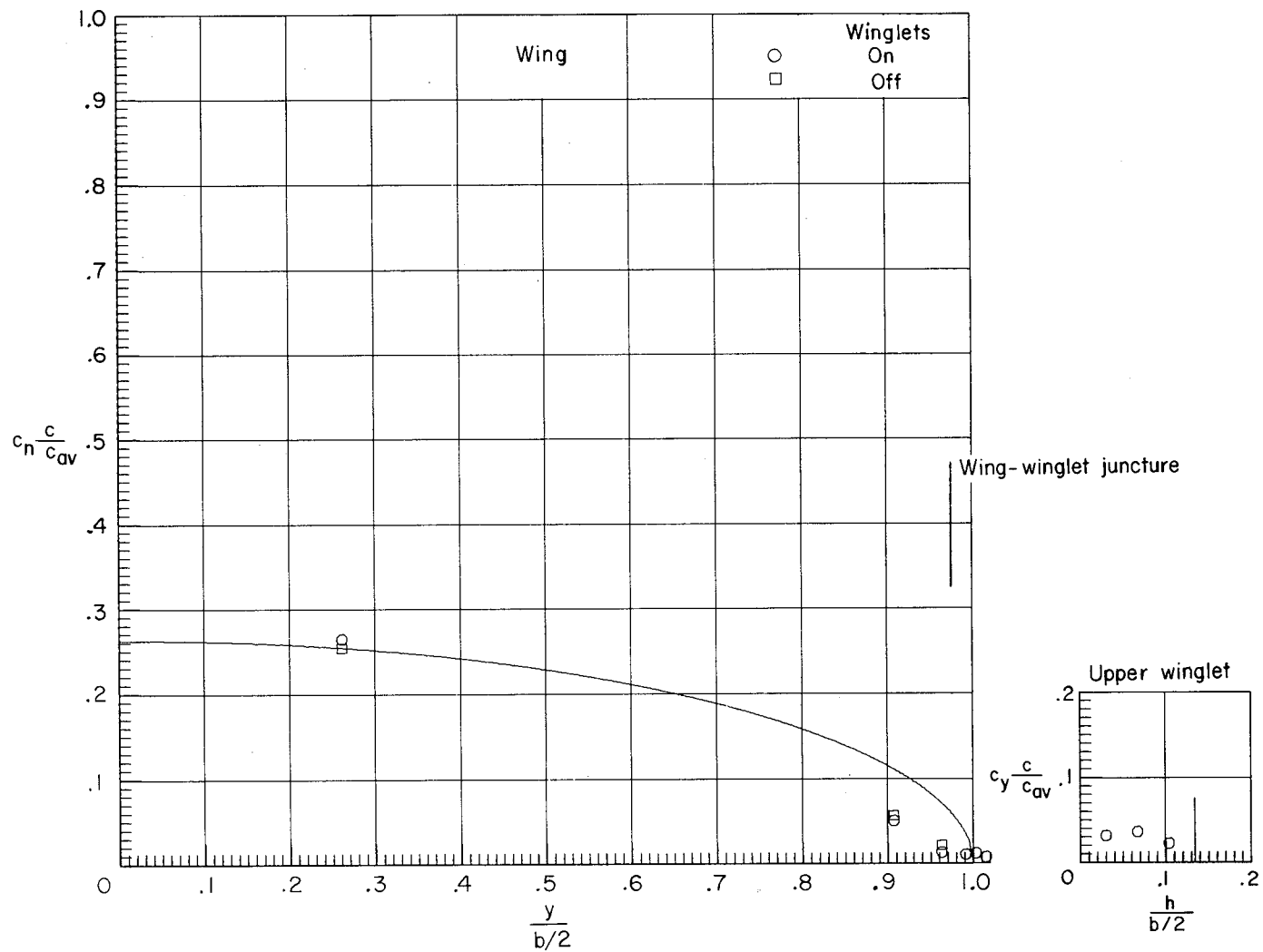
(f) $M_\infty = 0.800;$ $C_L = 0.18.$

Figure 9.- Continued.
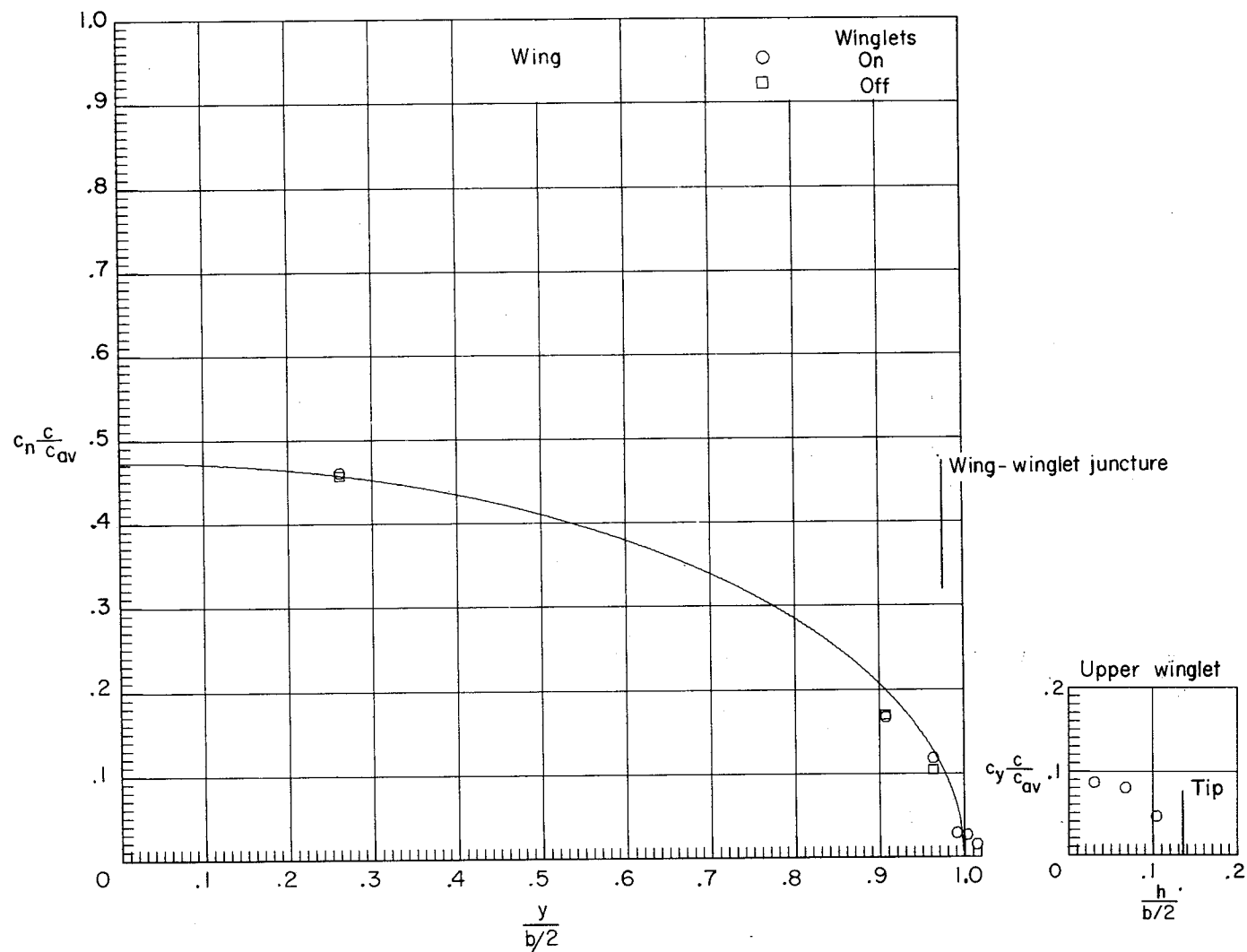
(g) $M_\infty = 0.800$; $C_L = 0.35$.

Figure 9.- Continued.
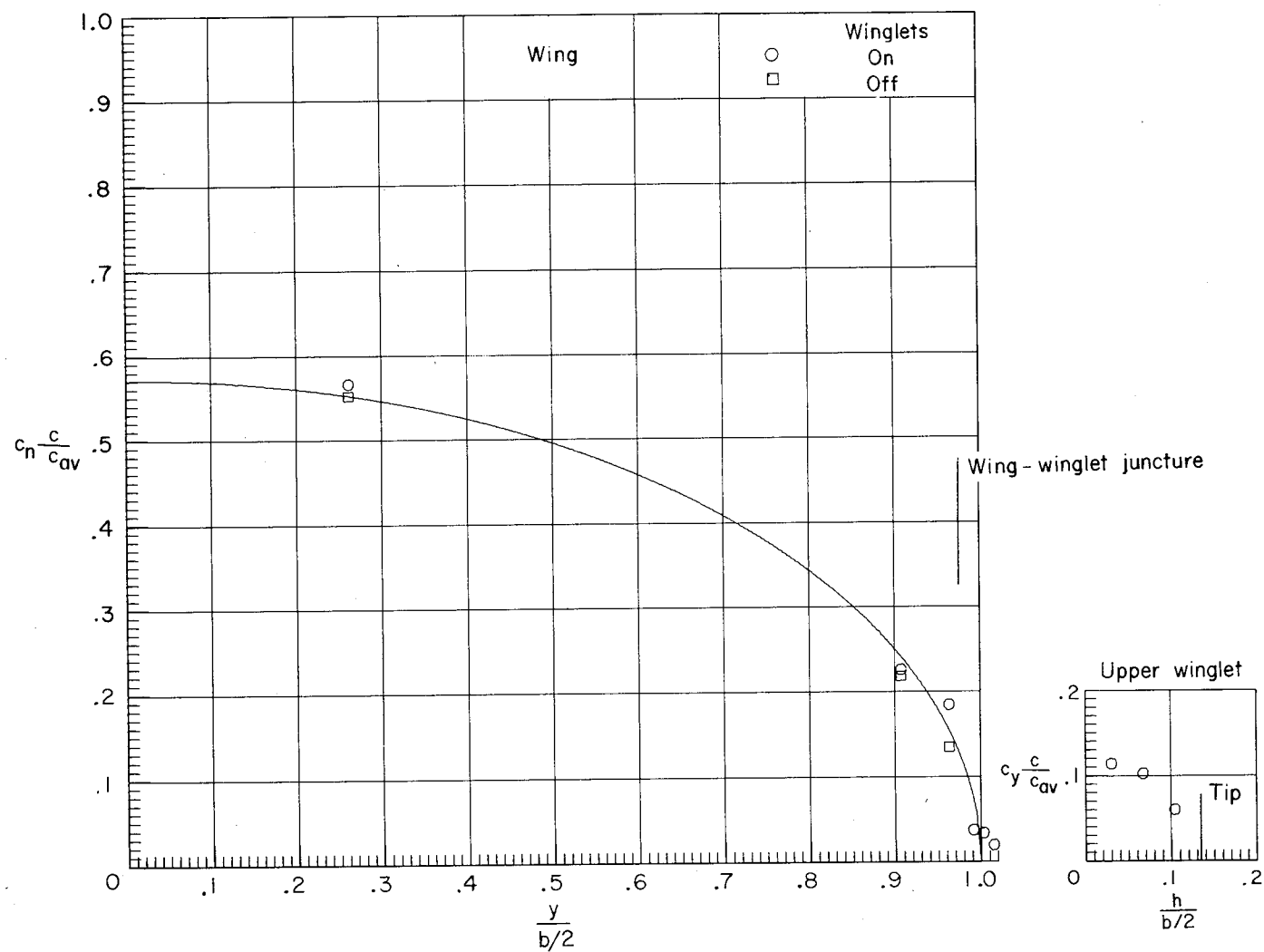
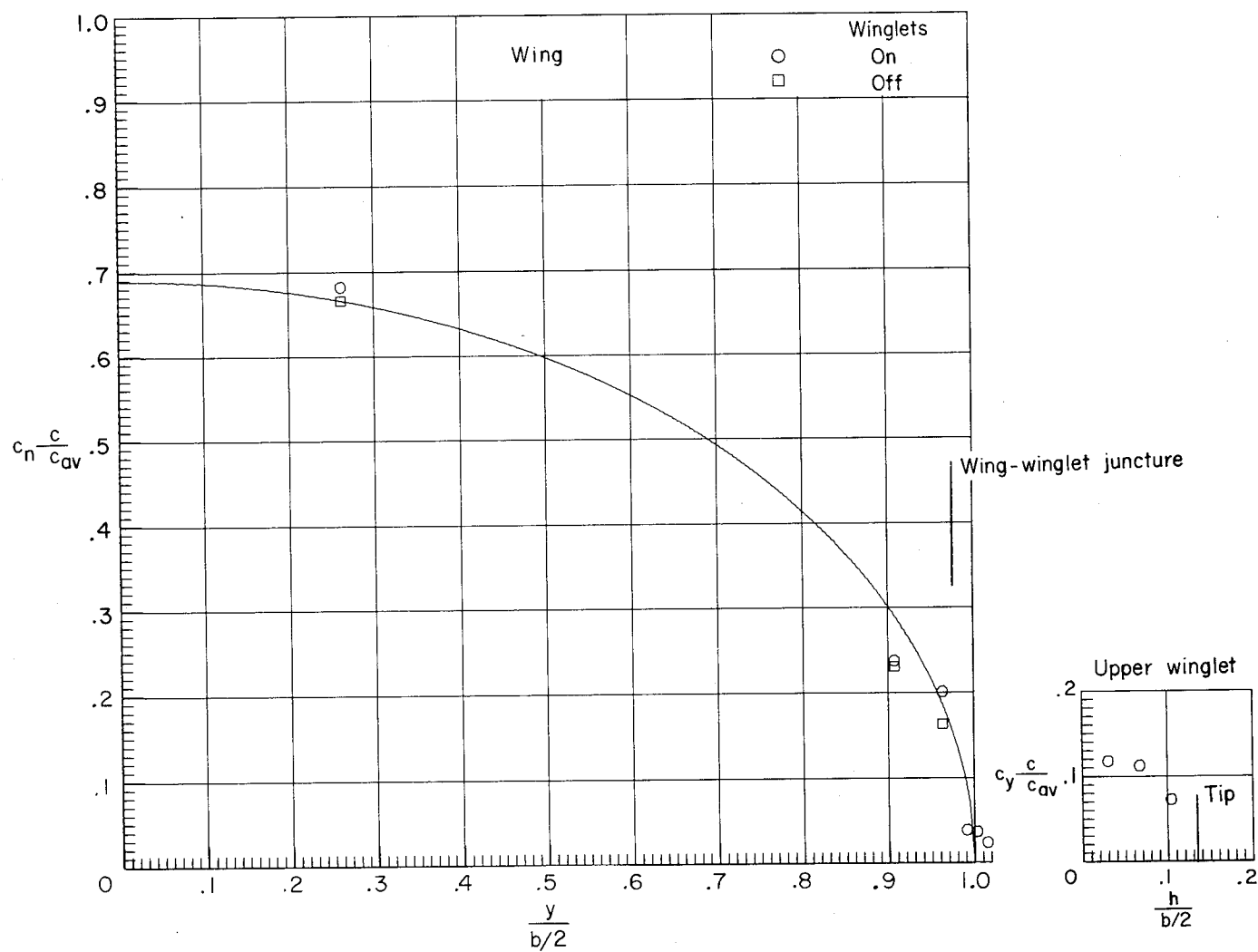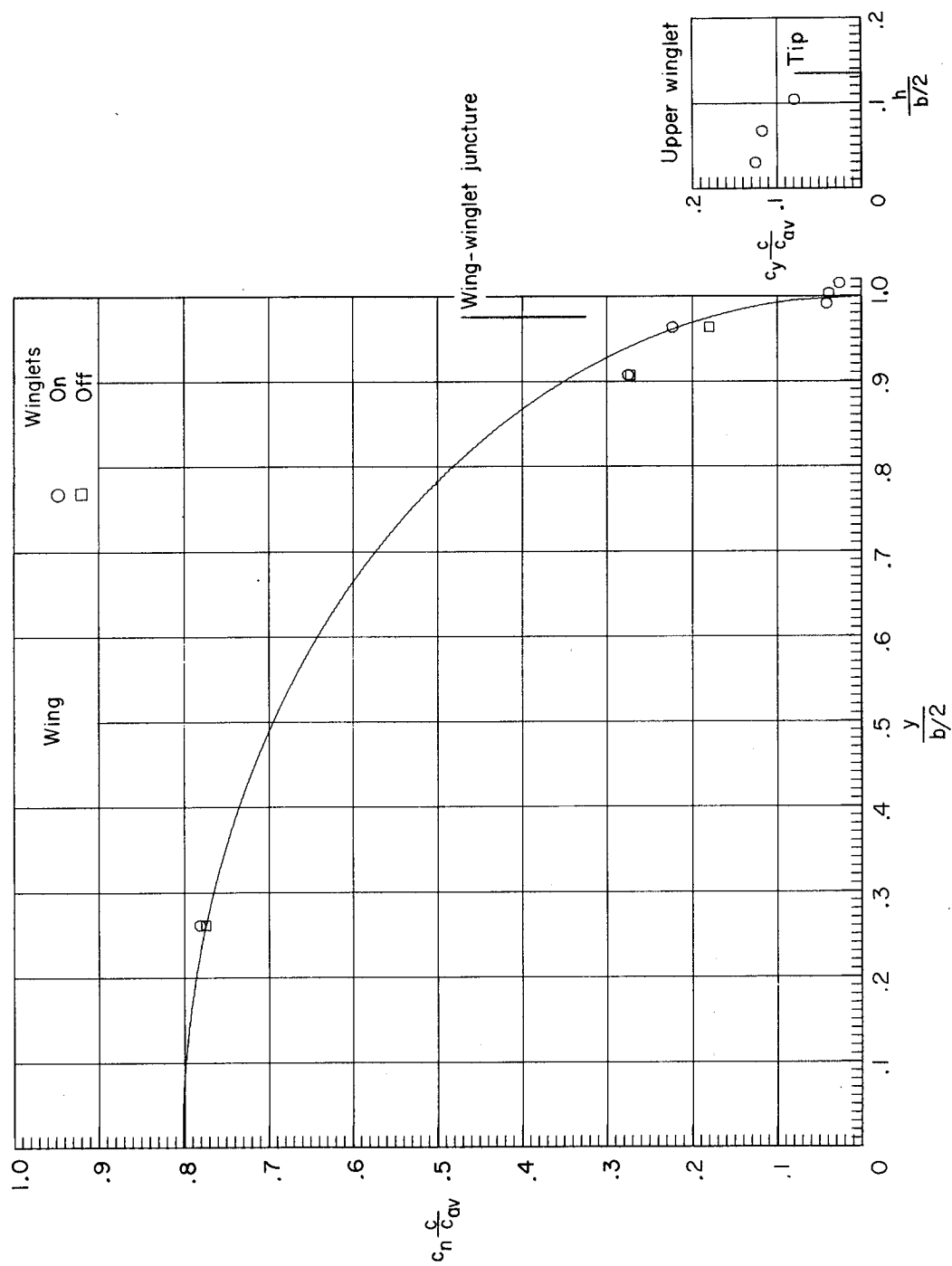(h) $M_\infty = 0.800$; $C_L = 0.44$.

Figure 9.- Continued.

(i) $M_\infty = 0.800$; $C_L = 0.54$.

Figure 9.- Continued.

(j)　$M_\infty = 0.800$;　$C_L = 0.61$.

Figure 9.- Continued.

(k) $M_\infty = 0.830;$ $C_L = 0.19.$

Figure 9. - Continued.

54
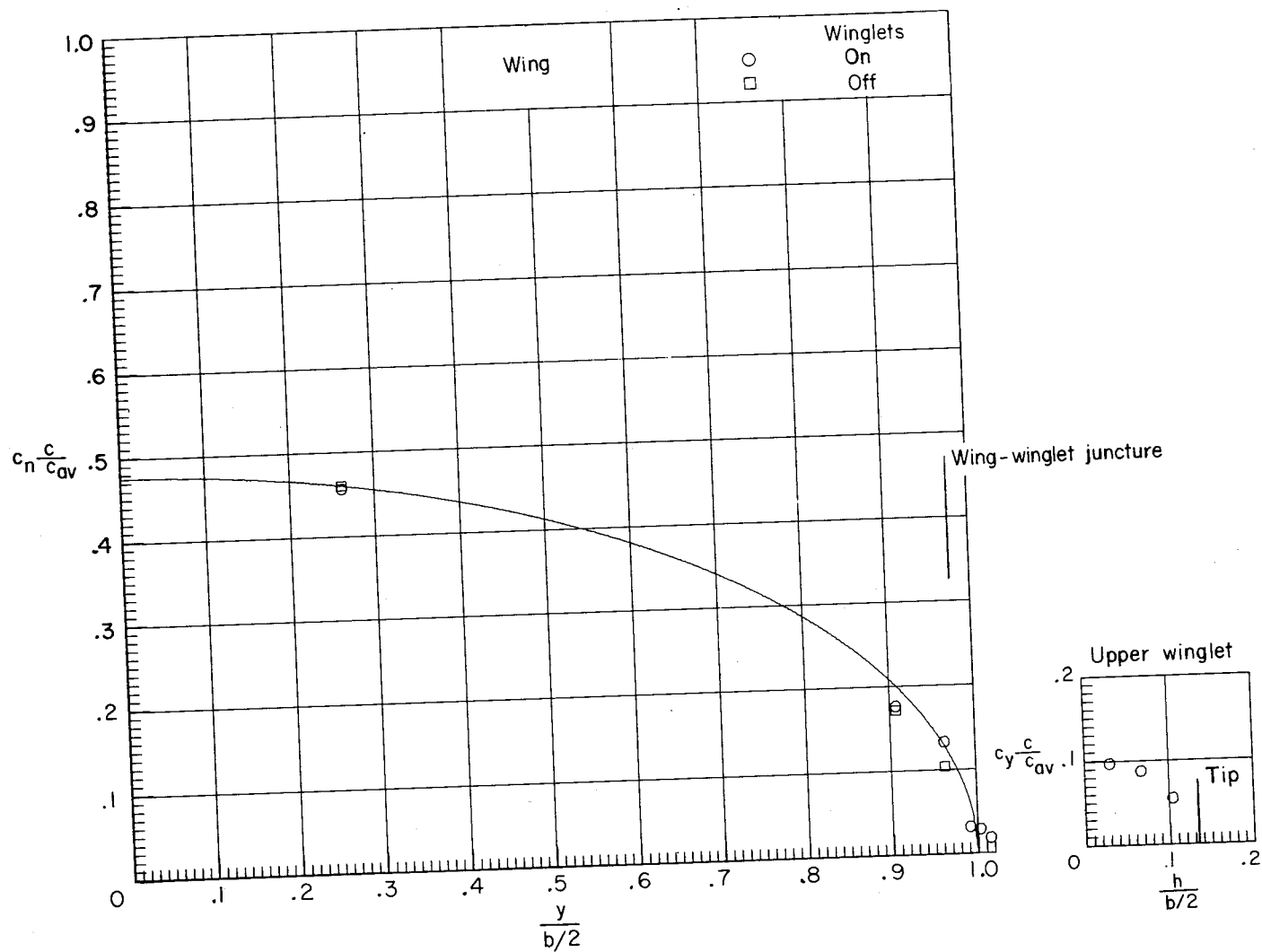
(1) $M_\infty = 0.830$; $C_L = 0.36$.

Figure 9.- Continued.
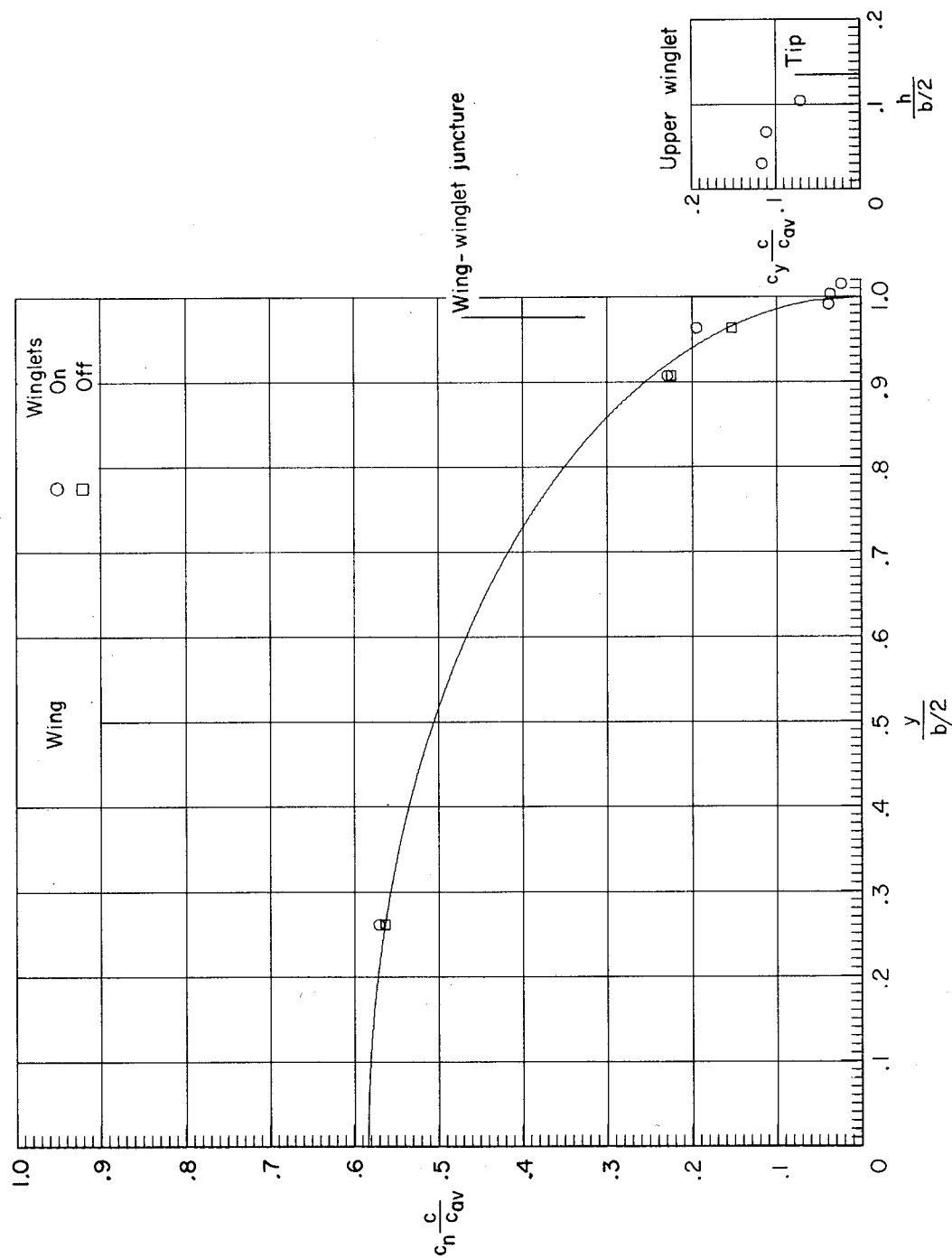
(m) $M_\infty = 0.830$; $C_L = 0.46$.

Figure 9. - Continued.

(n) $M_\infty = 0.830$; $C_L = 0.53$.

Figure 9.- Continued.

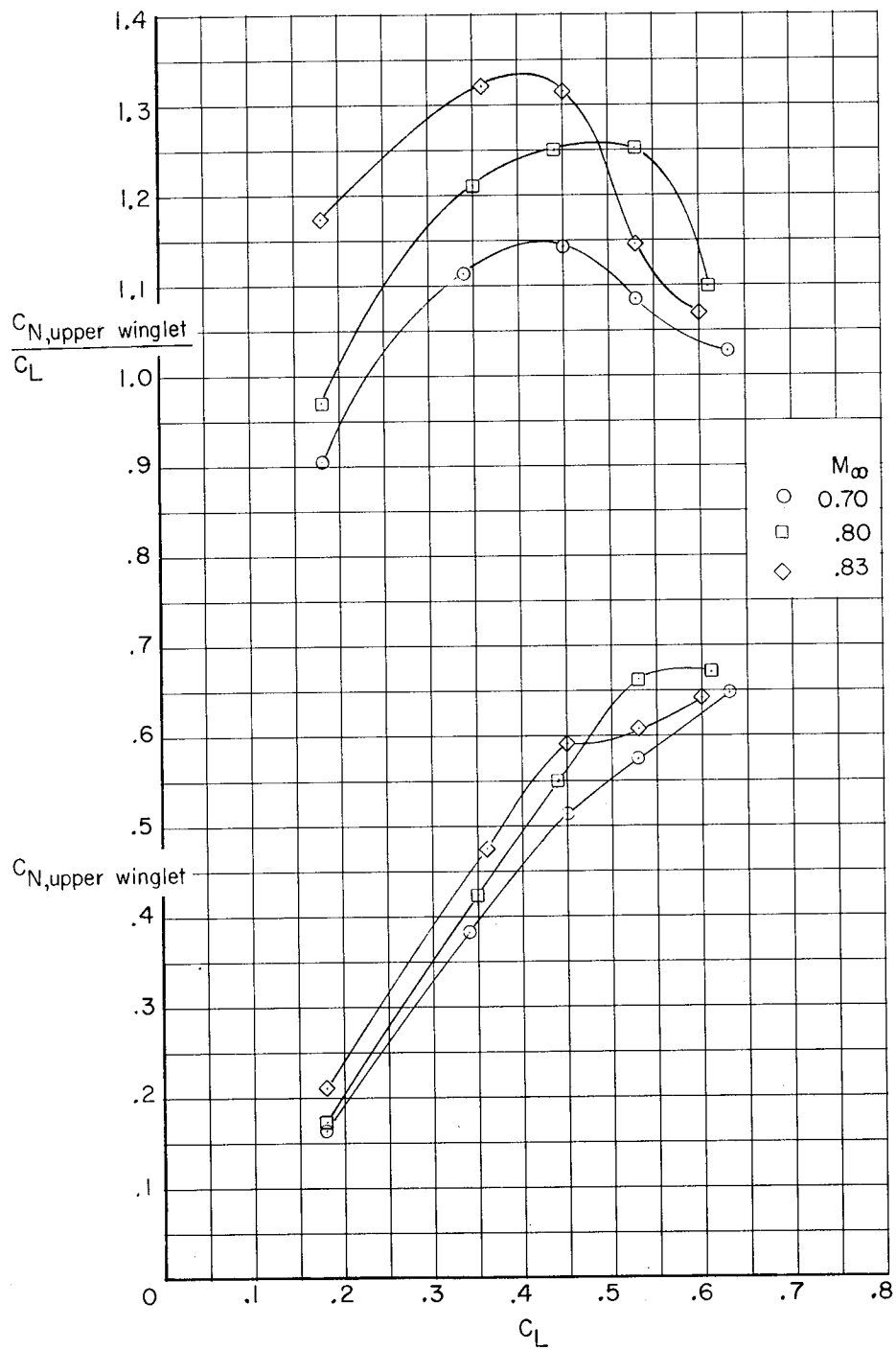(o) $M_\infty = 0.830$; $C_L = 0.60$.

Figure 9.- Concluded.
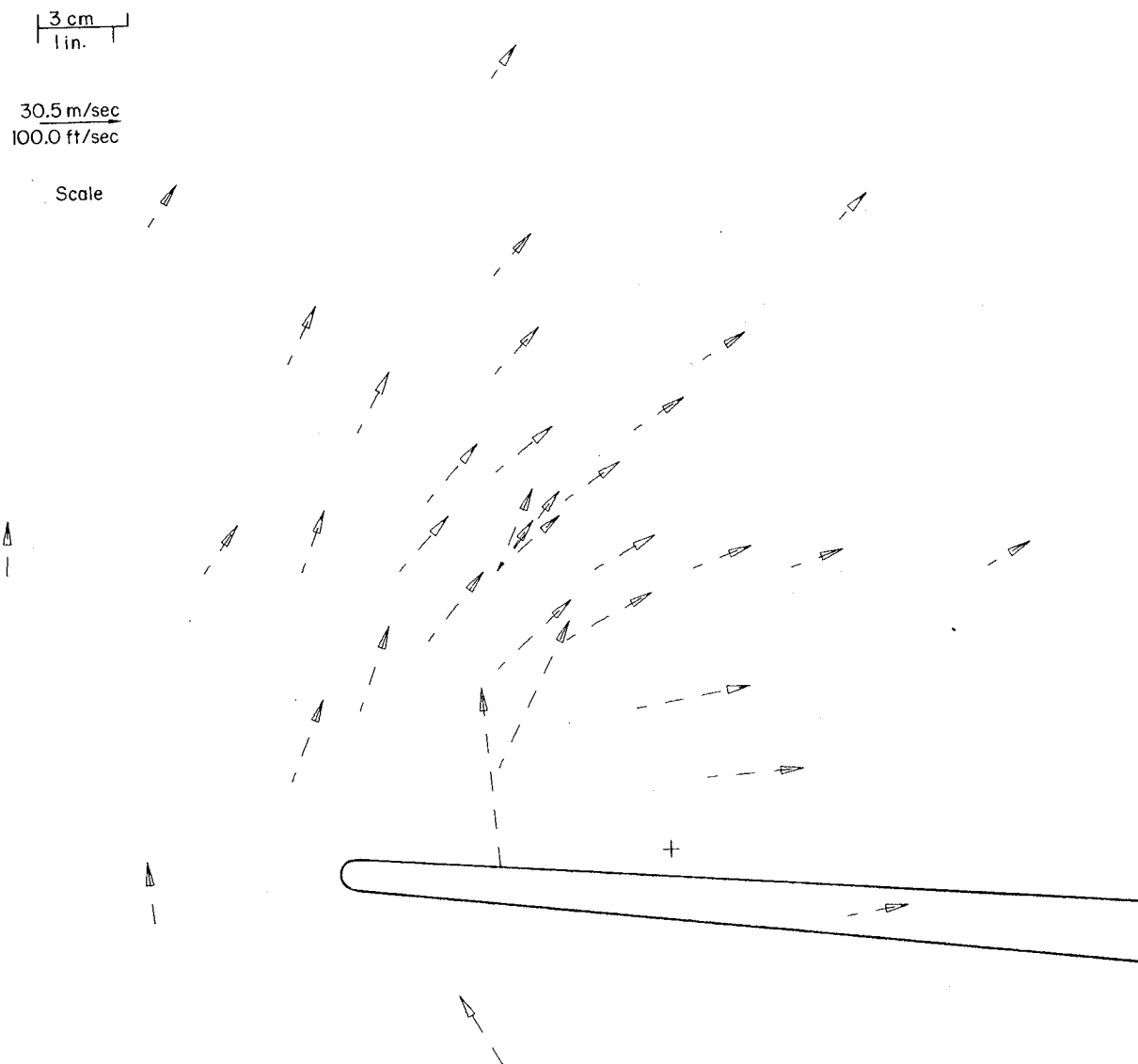
Figure 10.- Variation of upper winglet integrated normal-force
coefficient with lift coefficient.

3 cm
1 in.

30.5 m/sec
100.0 ft/sec

Scale

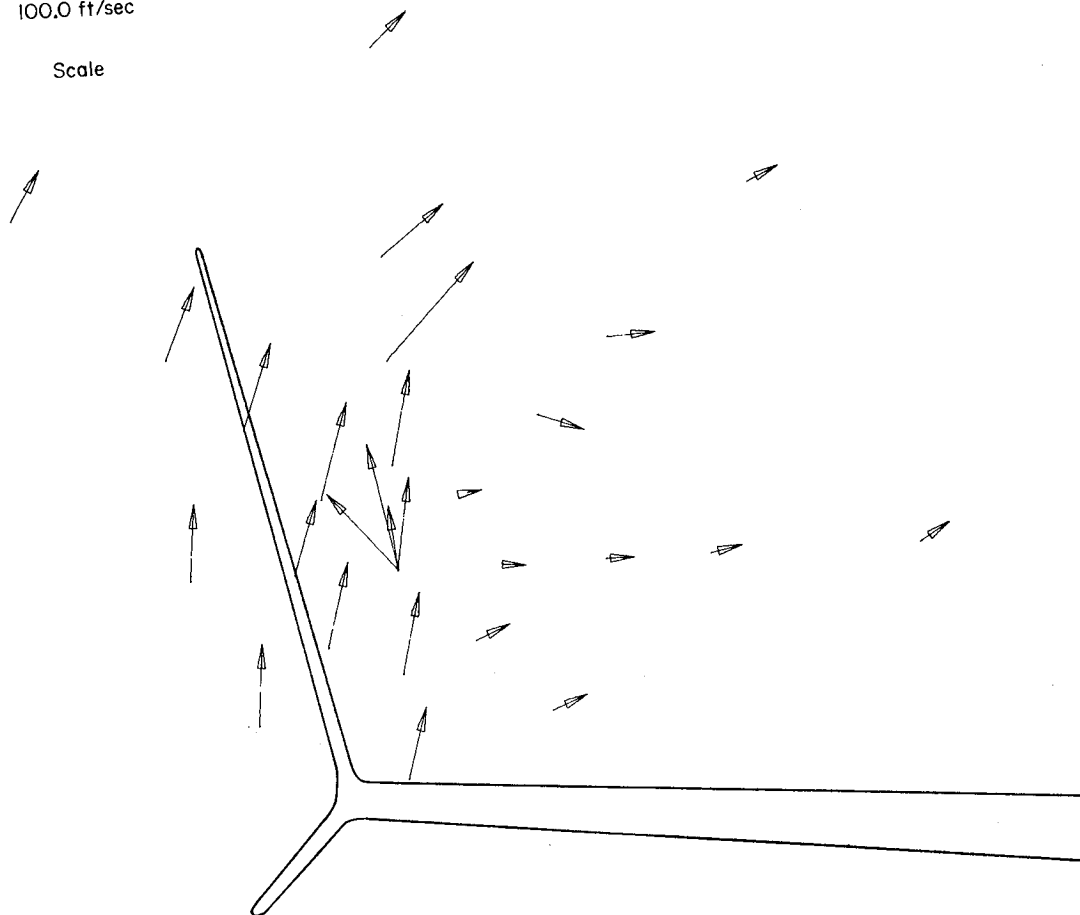(a) Wing with basic tip; $M_\infty = 0.700$.

Figure 11.- Flow-field crossflow velocity vectors behind model; $C_L = 0.53$.
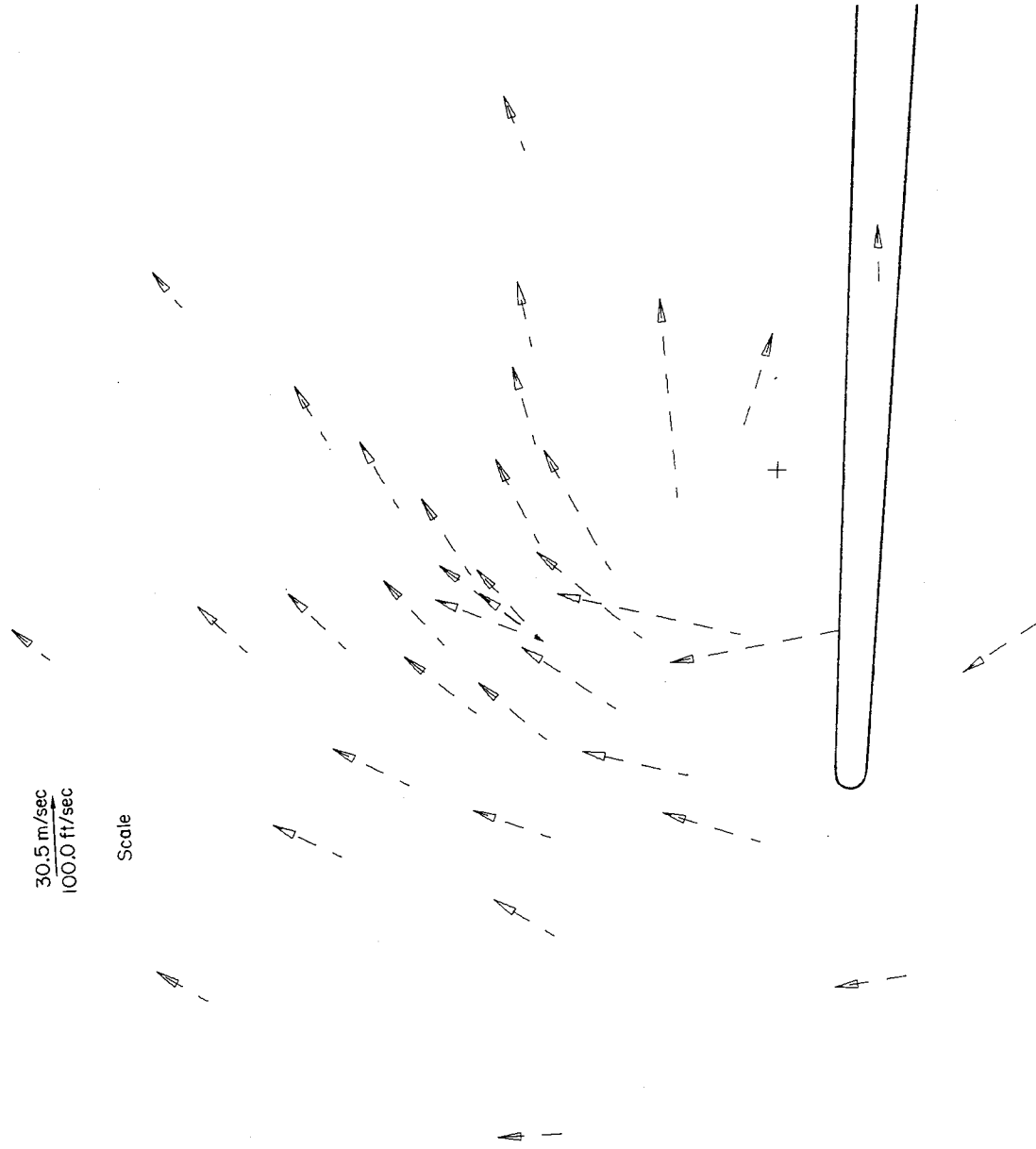
3 cm / 1 in.

30.5 m/sec / 100.0 ft/sec

Scale

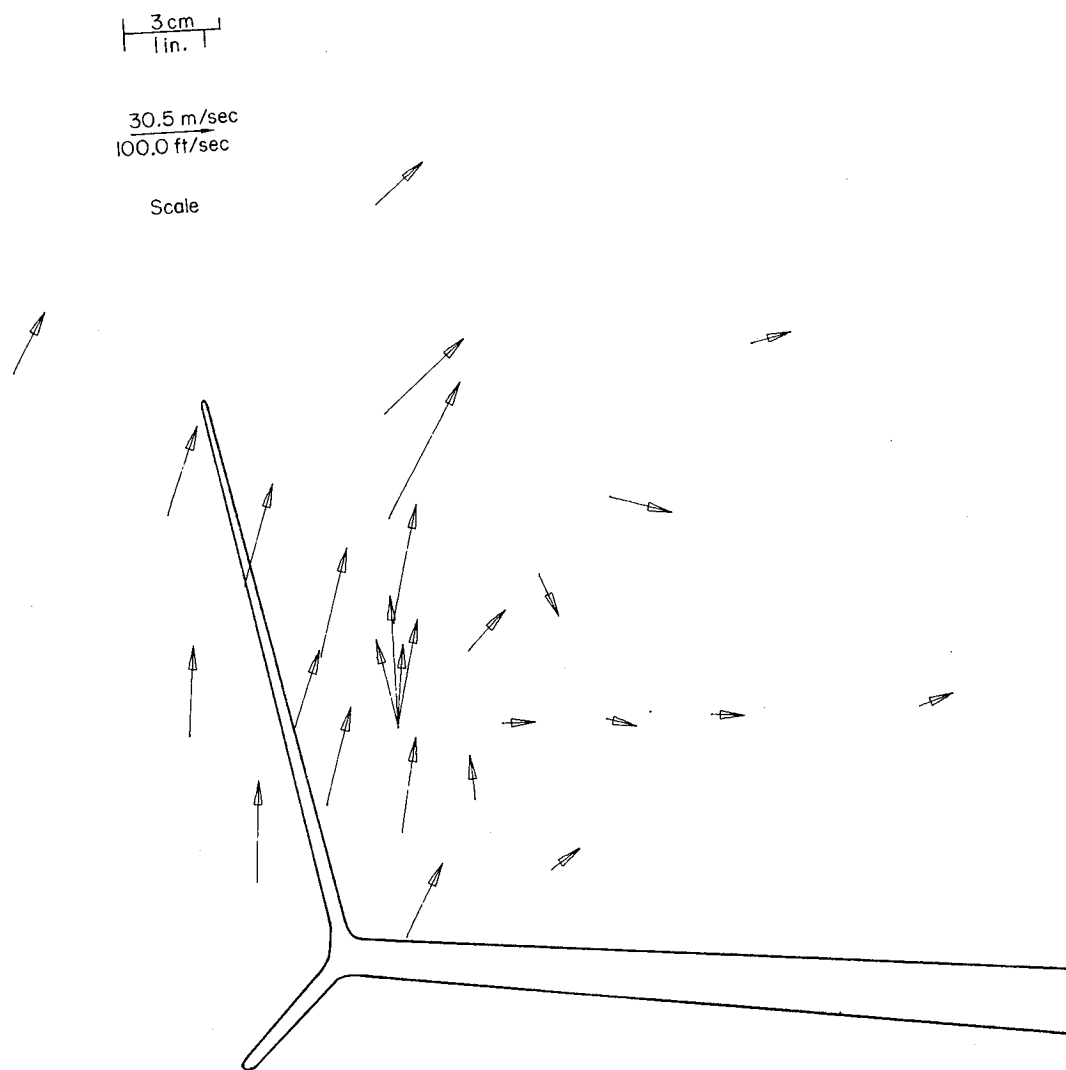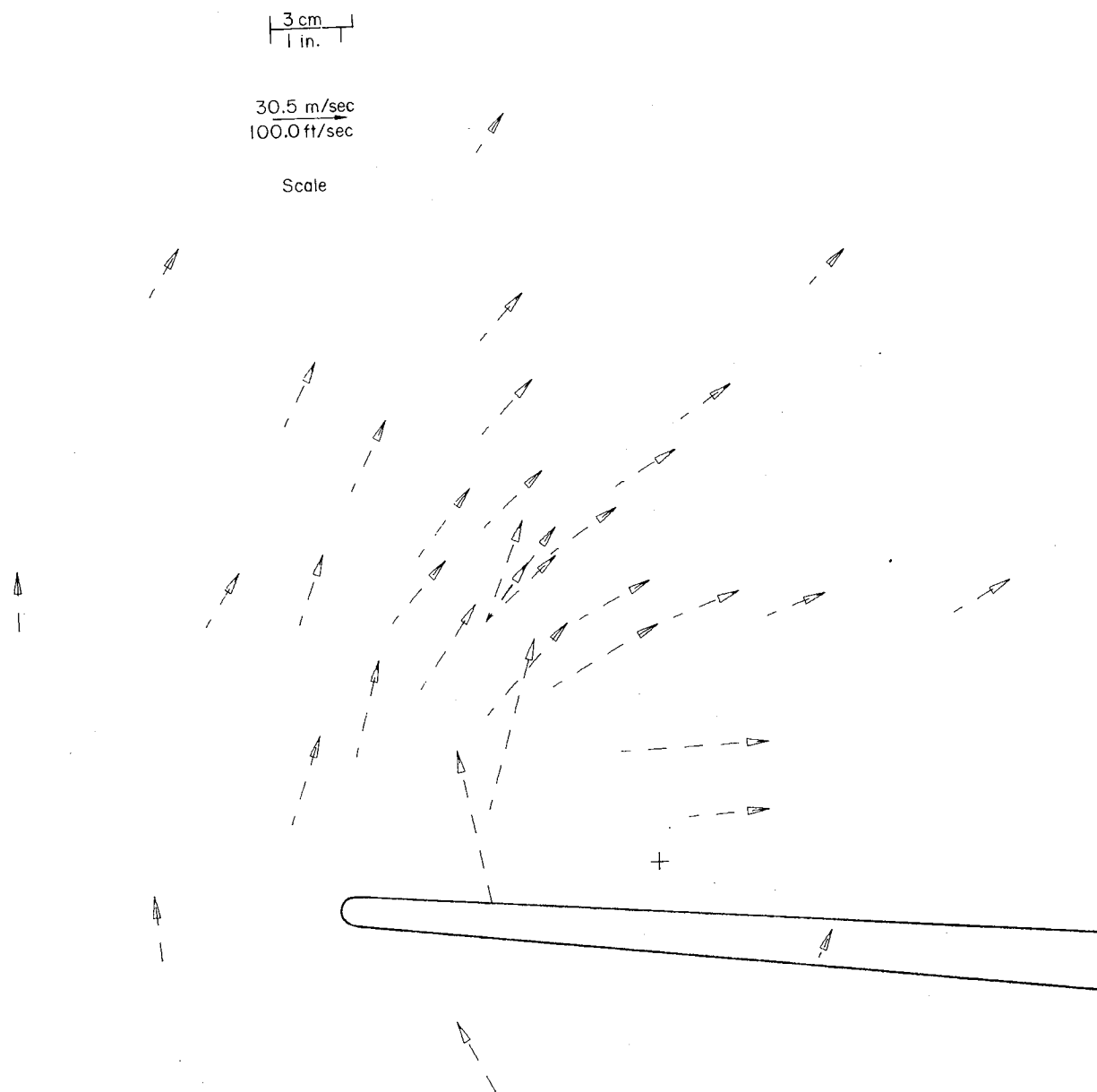(b) Wing with winglets; $M_\infty = 0.700$.

Figure 11.- Continued.

(c) Wing with basic tip; $M_\infty = 0.800$.

Figure 11.- Continued.

(d) Wing with winglets; $M_\infty = 0.800$.

Figure 11.- Continued.

3 cm
1 in.

30.5 m/sec
100.0 ft/sec

Scale

(e) Wing with basic tip; $M_\infty = 0.830$.

Figure 11.- Continued.

64

(f) Wing with winglets; $M_\infty = 0.830$.

Figure 11.- Concluded.
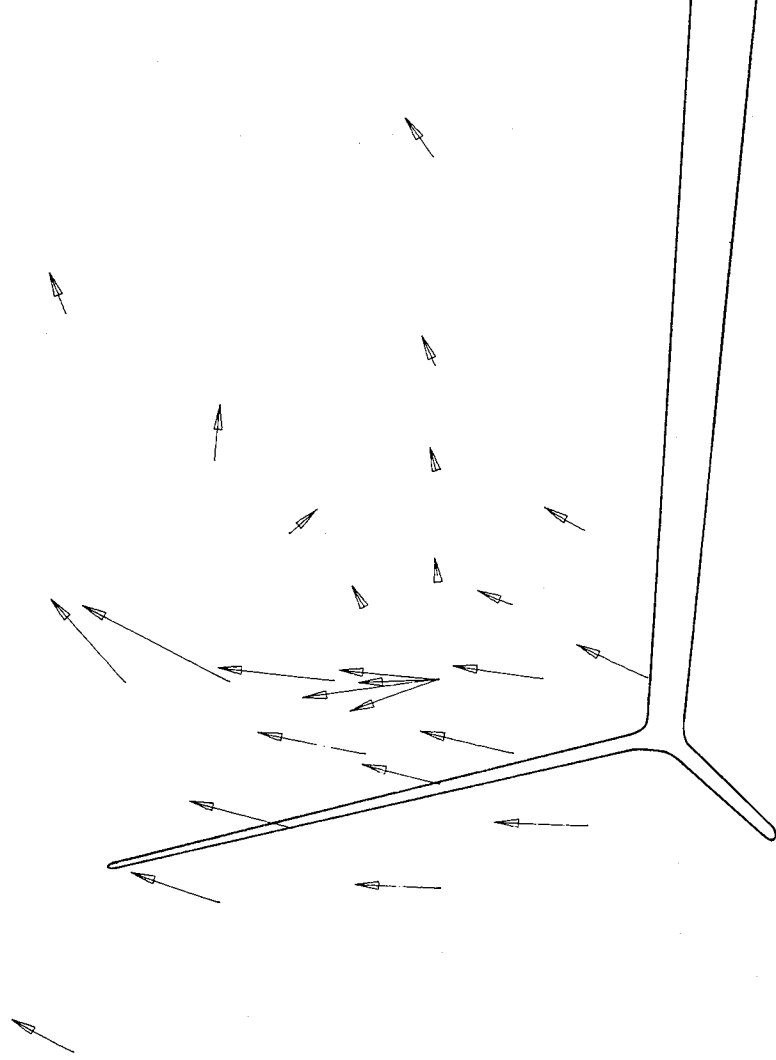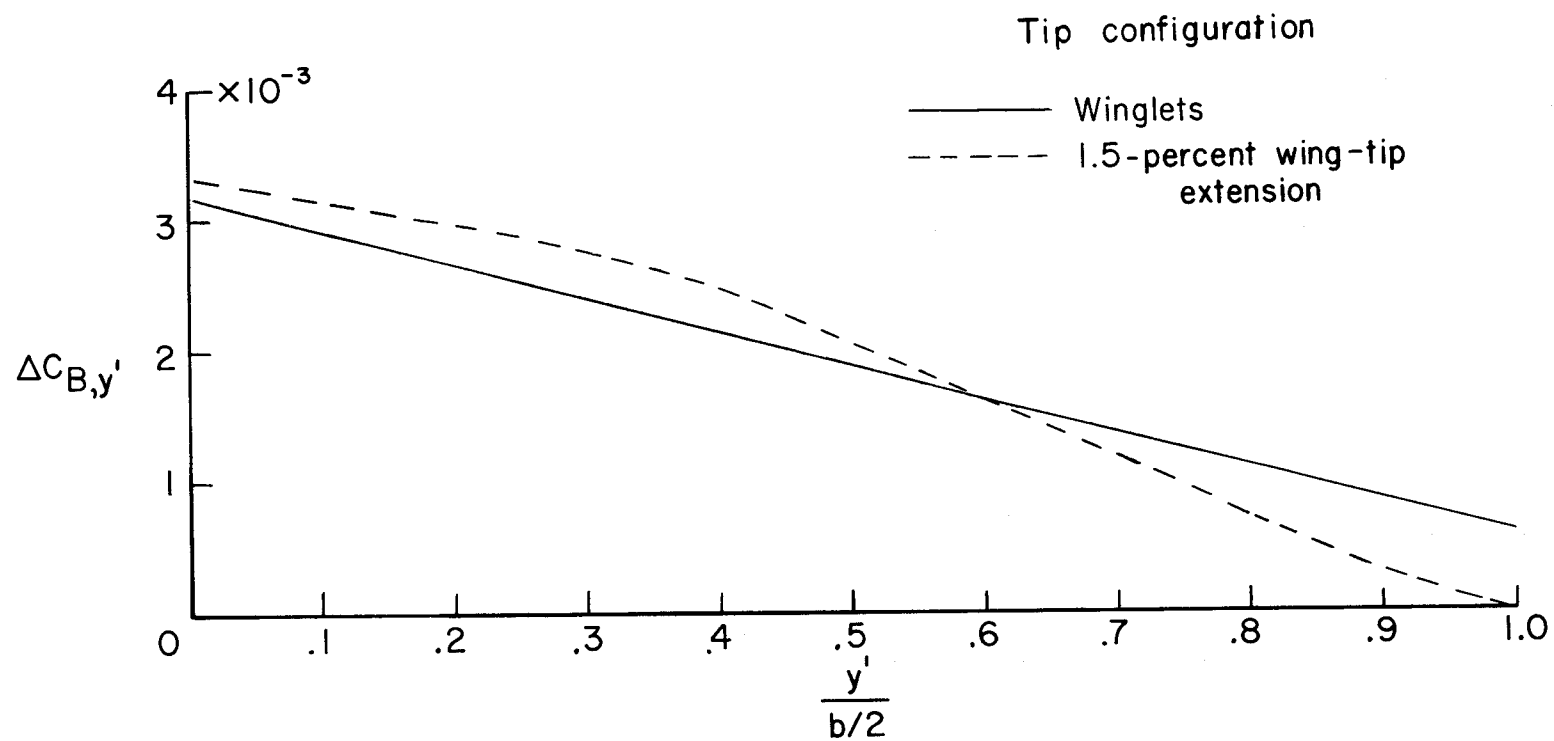
3 cm

1 in.

30.5 m/sec

100.0 ft/sec

Scale

Figure 12.- Comparison of bending-moment increments caused by adding winglets with those for 1.5-percent wing-tip extension for $C_L = 0.53$.

"The aeronautical and space activities of the United States shall be conducted so as to contribute . . . to the expansion of human knowledge of phenomena in the atmosphere and space. The Administration shall provide for the widest practicable and appropriate dissemination of information concerning its activities and the results thereof."

—NATIONAL AERONAUTICS AND SPACE ACT OF 1958

NASA SCIENTIFIC AND TECHNICAL PUBLICATIONS

TECHNICAL REPORTS: Scientific and technical information considered important, complete, and a lasting contribution to existing knowledge.

TECHNICAL NOTES: Information less broad in scope but nevertheless of importance as a contribution to existing knowledge.

TECHNICAL MEMORANDUMS: Information receiving limited distribution because of preliminary data, security classification, or other reasons. Also includes conference proceedings with either limited or unlimited distribution.

CONTRACTOR REPORTS: Scientific and technical information generated under a NASA contract or grant and considered an important contribution to existing knowledge.

TECHNICAL TRANSLATIONS: Information published in a foreign language considered to merit NASA distribution in English.

SPECIAL PUBLICATIONS: Information derived from or of value to NASA activities. Publications include final reports of major projects, monographs, data compilations, handbooks, sourcebooks, and special bibliographies.

TECHNOLOGY UTILIZATION PUBLICATIONS: Information on technology used by NASA that may be of particular interest in commercial and other non-aerospace applications. Publications include Tech Briefs, Technology Utilization Reports and Technology Surveys.

Details on the availability of these publications may be obtained from:

SCIENTIFIC AND TECHNICAL INFORMATION OFFICE

NATIONAL AERONAUTICS AND SPACE ADMINISTRATION
Washington, D.C. 20546